Double Degree Nanoquad Master Thesis

Coupling liquids with electronic excitations

Eva Panoni

ENS internship Supervisors:
Prof. Carlo Sirtori, Prof Lyderic Boquet
Polytechnic of Turin Academic supervisor:
Prof. Carlo Ricciardi
Université Paris Cité Academic supervisor:
Prof. Maria Luisa Della Rocca

JUNE 15, 2024
Paris

Contents

Theoretical introduction about quantum friction

The first seed for the begin of this internship, and the following PhD project, comes from previous works about a still mysterious water-carbon friction mechanism: up to now in the studies of solid-liquid interfaces, the former has always been picture as a passive external potential, with attention only on the friction resulting from static surface roughness of the solid. In few words what has been observed experimentally is that friction on graphite (Maali, 2008) is much stronger than the one register on monolayer graphene (Xie, 2018), tendency that is confirmed by also measurement with multiwall CNTs of different radius, with an abrupt increase of the slip length with decreasing dimension of the confining tube (E.Secchi, 2016). Such evidences suggested a possible link between hydrodynamic flow and the electronic dynamic of the confining material. It has to be said that none of these phenomenology is coherent with what MD simulations predict, it can be so deduced that a key ingredient is missing in the physical framework commonly used, which does not enable to capture some subtle mechanism going on at the interface, and this can be coming from the quantum dynamics of electrons in the solid.

The theory developed (N.Kavokine, 2022)explain the difference in between graphene and graphite hydrodynamic friction cases taking into account the different electron's dynamics of the two: the additional degree of freedom that electrons acquire in graphite (no more a 2D system as graphene) leads to the aperture of a band, whose width is determined by interlayer coupling strength and that leads ultimately to a very different low-energy excitation spectrum. In particular the solid excitation that is addressed is a low-energy surface plasmon mode, polarized perpendicularly to the stacking direction, which is believed to interact with liquid's charge fluctuations, dubbed "hydrons" (that give the water Debye mode,)-giving a non-negligible quantum contribution to hydrodynamic friction.

But also the different slippages for different radii CNTs can be understood in this perspective: again what changes is the interlayer coupling in the solid material, with big radii samples acting like graphite and the smaller like graphene, with nearly frictionless walls.

Phonon-drag mechanism for current generation

Strong from the above argument, we introduce here also a possible friction mediated current generation mechanism: the hydrodynamic friction, presented above, at the solid-liquid interface is transferring a momentum to the solid's phonons, these interacting with electrons, give the acquired excess of momentum to them. Naively the picture is the one of a "phonon wind" that "blows" over the Fermi sea, so electrons near the Fermi level will be dragged along the direction of the liquid flow, giving so rise to an electrical current. In the following a sum up schematic

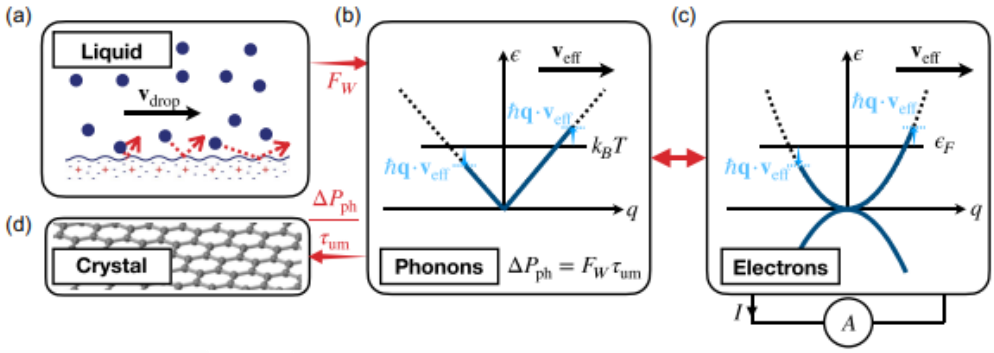

Figure 1 Phonon drag mechanism: momentum balance, propagation of asymmetry in the distributions. Diagram representing the momentum fluxes in between four subsystems in which the solid-interface one is divided. Naively the liquid acts as a momentum source and the solid's crystal as a momentum sink. The phonons (electrons) accumulate a momentum $\Delta P_{ph}(\Delta P_e)$ corresponding to a Doppler shift of $\hbar q v_{ph}$ ($\hbar q v_e$) of their momentum distribution. (B. Coquinot)

Theoretical framework semiconductor's plasmons

In this chapter we propose a study of optical properties of thin highly doped semiconductor layers (degenerate doping, Fermi level lying above the conduction band minimum) in the infrared spectral region. Thanks to the high levels of doping and so high electron densities, collective oscillations of the electronic gas, start to dominate, leading to the appearance of a so called "Berreman mode". This is a volume plasmon not to be confused with surface plasmon polariton (the mode indeed is resonant near the plasma frequency) (A., 2007)

Giving a naïve description of the physical picture, we know that when light shines on a bidimensional gas, interaction between this one and electrons, gives rise to intersubband polarization along the growth direction of the well. the mentioned polarizations are associated to the intersubband transitions of the well, that can be picture in mind as dipole oscillating at a frequency characteristic of the transition (spacing in between the energy level).

a) b)

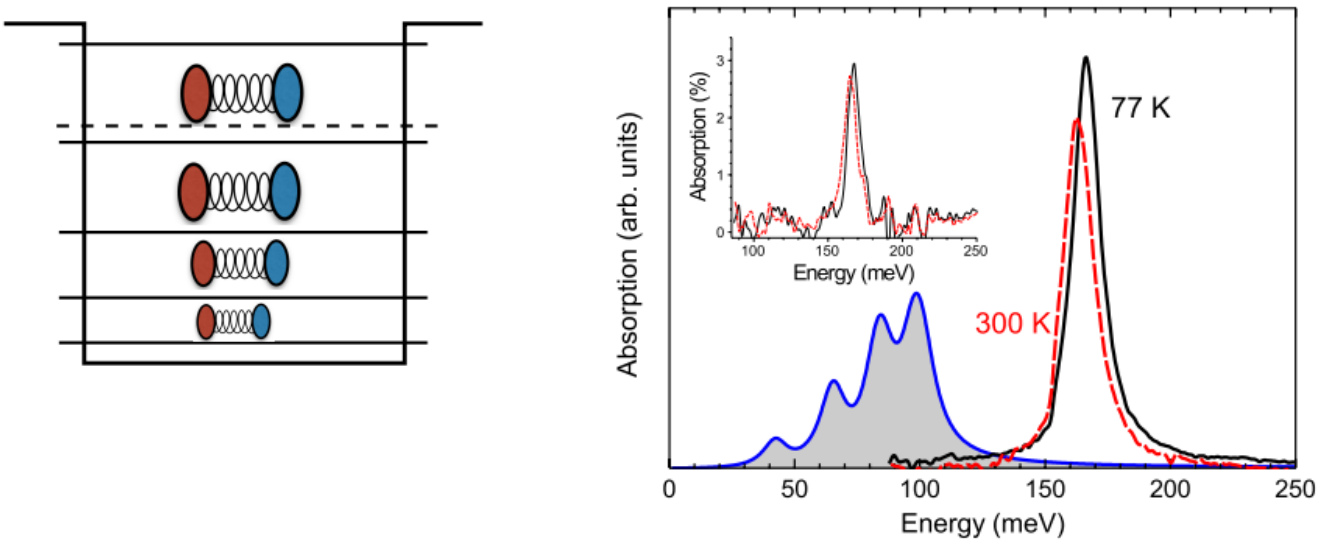

Figure 2 a) Schematic representation of the intersubband transitions as oscillators characterized by different strengths b) Absorption spectra of a 18.5nm quantum well GaInAs/AlInAs. The inset presents spectra measured on the sample at Brewster angle. The blue line in the main panel represents the simulated absorption spectrum, resulting from a single-particle description and Lorentzian line broadening of the allowed transitions. (Pegoletti)

From a single particle description, the adsorption spectrum should appear as a collection of overlapping peaks, at the frequencies correspondent to that of the allowed transitions. The responses of the independent and incoherent oscillators, should sum up to give a spectrum with a very broad feature. What instead is observed, and confirm indeed the "collective" nature, is a single sharp resonance peak, no trace is present of the transitions between electronic energy levels. The physical microscopic interpretation is that the electronic density is so high, that the Coulomb dipole-dipole interaction is inducing a coherence effect, such that all dipoles are oscillating in phase in an unique high energy mode (in case of strong doping indeed at an energy that is far apart from those corresponding to the single bare transitions), each of the transitions concentrate in it their respective oscillator strength, so that the entire system's answer is characterized by a single frequency.

Moreover, a subtle observation that could have been made is that because of the very intense doping level and the non-negligible non parabolicity in some way it would be expected a broadening of the linewidth of the peak, instead this stays comparable with the typical ones of inter-subband transitions alone measured in modulation doped samples, it seems that this many body optical resonance, arising from a collective effect is like protected from disorder.

Interesting is to point the exotic coupling of this matter excitation with electromagnetic field. Generally speaking, in the world of quantum electrodynamics, the terms strong and ultra strong coupling regime are used in the case in which the interaction cannot be described by usual perturbation theory. Such particular condition is usually achieved by matching a material excitation with strong oscillator strength and a spatially confined electromagnetic mode (use of an optical microcavity). Surprisingly in the case of our plasmon excitations, no optical confinement is needed to reach such regime, since the coupling between the material excitation and free-space radiation is already itself very intense. A parameter that helps us to quantify the strength of the interaction is the radiative decay rate, usually this is much smaller than the nonradiative one, meaning that the electronic excitation dissipate energy with a much greater speed respect to the one with which are excited. But for the Berreman mode in particular condition this no more holds, and we the interaction with free space radiation ca be so intense that the radiative live time is much greater than the non radiative one.

The total decay rate, or linewidth, of the Berreman mode is:

$$\Gamma_{tot} = \gamma_{nr} + \Gamma_{rad}(\theta, \omega)$$

Where the expression of the radiative contribution is the following

$$\Gamma_{rad}(\theta, \omega) = \Gamma_0 \frac{\omega}{\omega_0} \frac{\sin\theta^2}{\cos\theta}$$

This last expression comes from the solution of Langevin equations in the input-output formalism: in such physical picture the plasmon excitation is descried as coupled to two bosonic baths, on one side the electromagnetic free space radiation, like a photonic reservoir, and on the other an electronic reservoir, the coupling of the plasmon excitation with each of them is described respectively by $\Gamma_{rad}(\theta, \omega)$ and γ_{nr}, parameters that rapresnet the decay rates for these two competing channels. In other words, when the non radiative lifetime is greater than the radiative one is more favourable for the plasmon to "relax" down in the into the electronic bath, or better they decay into the electronic bath at a faster rate than they are excited. In the opposite case, when the radiative lifetime is greater than the non radiative one, plasmons are excited at a peace faster than the one they could relax into the electronic bath. So depending on the relation between the two decay rates one path is dominant over the other one, decay in the photonic bath or electronic one.
The same expression, without a frequency dependency, can be obtained as spontaneous emission rate of the plasmon mode using perturbation theory with Fermi's Golden rule:

$$\Gamma_{rad}(\theta) = N_s \frac{2\alpha}{m^*} \frac{\pi\hbar}{n} \frac{sin\,\theta^2}{cos\,\theta} \quad (1)$$

Importantly it has to be pointed out the proportion with the areal electronic density and the strong dependence on the incident angle (always the internal one), this latter takes into account the effective interaction of light with the sample considering the angle of incidence and effective length: only interaction with p-polarized light, that is to say only the component of the electric field oriented along z-growth direction $Ez = E_0 \sin\theta^2$, where the squaring is coming from the fact that the absorption is related to the intensity signal, and that the effective length "explored" goes like $\cos\theta^{-1}$
At different angle you obtain the dominance of one relaxation mechanism over the other: for small angles the angle dependent term is very small, meaning that for very small incident angles the linewidth is dominated by the nonradiative mechanism, which is non angular dependent, moving to wider angles the radiative route is the most favourable one and a broadening of the resonance is expected.

Simulation details

The formula here proposed as well as all the simulation code used is based on a quantum model that can be applied to any arbitrary confining potential, perfectly reproducing the experimental adsorptions spectrums.
Furthermore allows the study of the interplay between Coulomb interaction, determining the coupling between intersubband plasmons, and quantum effects such as the confinement one, making possible to investigate the possibility of engineering new quantum structures based on collective excitations.
In order to compare experimental and theoretical absorption spectra, also numerical simulation have been performed. In particular we have make use of a C++ code, implemented previously by G.Pegoletti, to calculate the adsorption spectra, modelling the systems under study as perfectly square wells and so defying the consequent band structure on the base of Kane model. the tuning parameters for the simulation were the material composition, and so the potential depth, well dimension and doping level. The target elements were the resonance energy of the plasmon, as well as the linewidth of the Lorentzian like peaks, together with their angle dependence.

Samples description

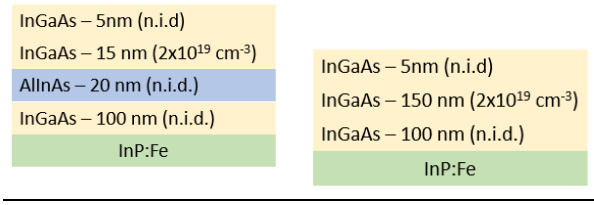

Figure 3 schematic of the samples. samples were grown via Metal Organic Chemical Vapor Deposition (MOCVD) on an InP substrate by the team of Grégoire Beaudoin, Konstantinos Pantzas, and Isabelle Sagnes at the Centre de Nanosciences et Nanotechnologies (C2N) in Palaiseau, France.

The first sample studied consists of a 150 nm layer of InGaAs doped nominally with $Nv = 2e19\ cm^{-3}$ grown between two not-intentionally-doped InGaAs layers. In the second case the doping level is still the same, but the thickness of the doped slab is reduced of one order, with the addition of a barrier of AlInAs, to ensure the strict confinement of such case.
Our semiconductor samples, featuring a highly doped layer right at the top, present a unique scenario. Instead of being buried within the substrate, the doped layer is exposed directly to the air. This configuration allows the plasmon confined in this layer to be easily accessible and interact directly with any liquids and their excitations. This direct interaction positions our plasmons as ideal candidates for exploring the mechanisms of energy or momentum exchange between water excitations and electronic ones. To optimize this coupling, electrons must be confined at the liquid-solid interface. Given is 2-dimensinal nature, graphene is a perfect candidate to explore the cross-coupling between liquid and electronic excitations. However, our plasmonic structures, where the doped layer could be in direct contact with the liquid, also meet the necessary criteria for liquid solid studies. Plasmons are therefore a versatile candidate to "talk with water hydrons".

Measurement strategy: transmission FTIR spectroscopy

For this one we have measured the transmission spectra for the two different polarization of light p and s modes using a Fourier Transform Interferometer (FTIR), a black body source, and a liquid nitrogen cooled mercury cadmium telluride (MCT) detector. For each angle and each polarization the light signal has been acquired incident light on two separate regions of the sample: one with the highly doped layer, "active" one, and another in which the layer has been etched away, remaining so only the substrate, "reference"

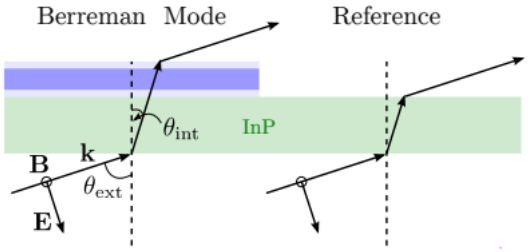

Figure 4 schematic of the measurement technique simple transmission (Haky, 2022)

As already from the previous theoretical introduction can be understood, it is expected that only p-polarized light (TM mode) can interact with the plasmons, this indeed has an electric filed component fully perpendicular to the plane of the quantum well (along the grow direction), so aligned with the transition dipole moment (by contrast s-polarized light has an electric field entirely in the plane of the structure, cannot so interact with the z-oriented dipoles of the material).
In the analysis of the spectrums collected attention has to be paid to the fact that the Fresnel coefficients have a certain dependence on the angle of incidence and polarization of light, moreover some artifacts can be introduced by the optical elements, also them could present slightly different response for different light modes. For this reason the spectrum obtained never have a baseline of one, for compensate for such effect, the data are further normalized by the ratio of p and s polarized spectra from the transmission signal through the substrate.

$$\frac{T_{active}(p)\Big/T_{active}(s)}{T_{substrate}(p)\Big/T_{substrate}(s)}$$

At an incident angle of 72° (18° internal angle) no p-polarized light is reflected back, this indeed correspond to the Brewster's angle for air/InP interface, in other words the angle for which the reflection coefficient for p-polarized light goes to zero.
Thanks to this the absorptivity of the media can be easily extracted from the experimental data for this particular angle as 1-Transmission (after correction of the baseline through normalization).
In the following attention has to be paid in distinguish between external and internal angle of incidence, indeed due to the large refractive index mismatch at the air/InP interface the angles of incidences inside the semiconductor are much smaller than the external ones.

Results for 150nm doped layer

In the first panel the bare transmission spectra acquired focusing the beam on the etched and non-etched part of the sample, here indicated with the names "substrate" signal and "active" signal. And for each of them, through the use of a polarizer, placed at the exit port of the FTIR, we select p or s modes.
The resonant peak is observed at 168meV.
Since for this structure no confinement effect is expected, the Berreman mode should manifest itself at the classical plasma frequency, for this reason, taking into account the nonparabolicity in the evaluation of the effective mass, a first estimation of the electronic density can be retrieved (w_p^2[1] $= \frac{N_v e^2}{m^* \epsilon_0 \epsilon_\infty}$).

a)

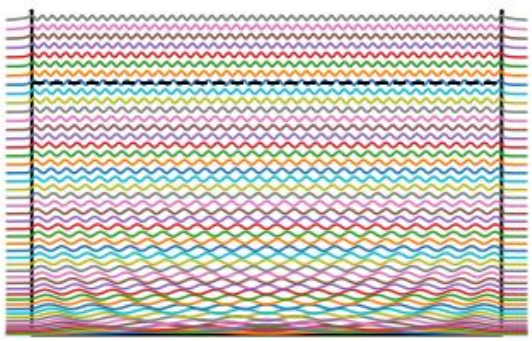

b)

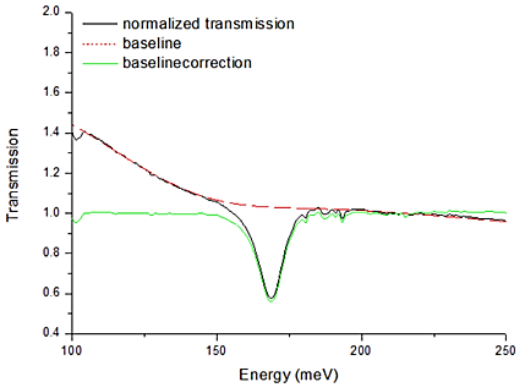

Figure 5 a) square moduli of bound electronic states plotted at their respective energies in the square potential b) baseline correction for Brewster angle

[1] ωp is sometimes called the screened plasma frequency since ε∞ has been (arbitrarily) included in the definition, the ∞ subscript is used to denote that this dielectric constant is valid at frequencies much greater than ωp.

a)

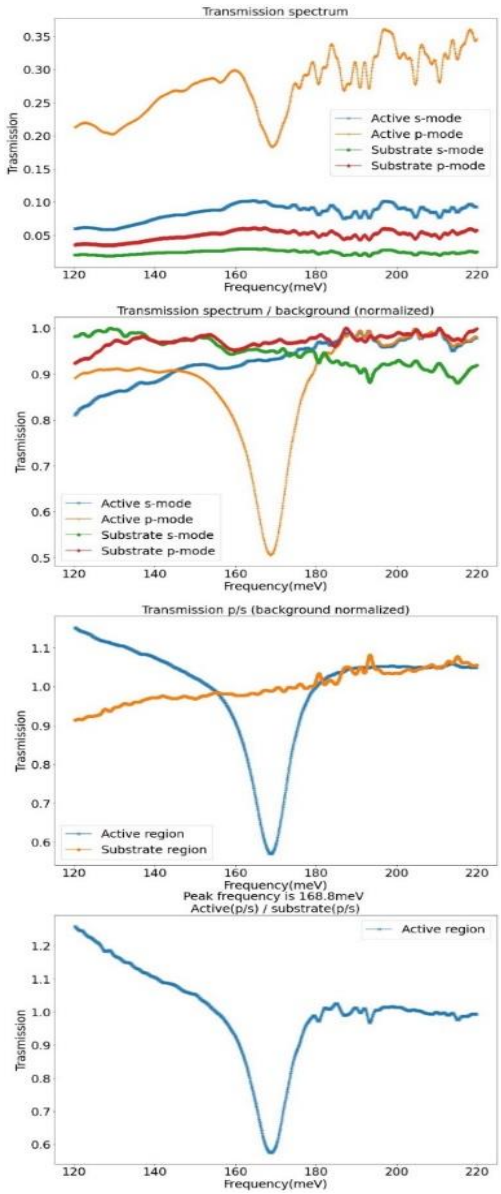

b)

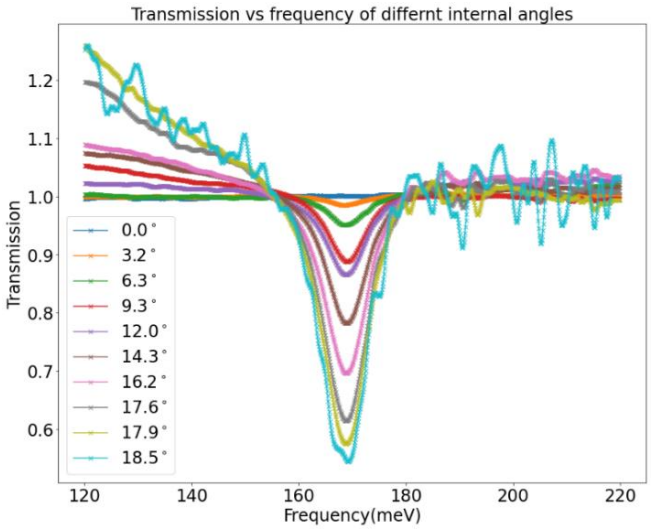

c)

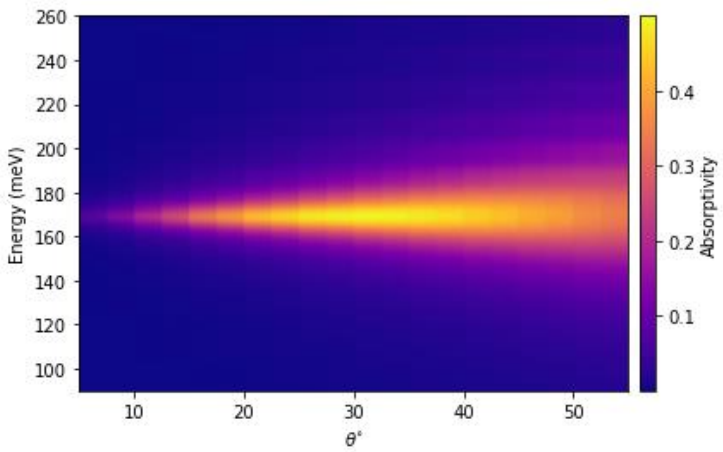

Figure 5 a)Transmission spectra acquisition. "Background normalized": FTIR signal, without the sample, was done at the beginning of the measurement, this just contains features coming from the source itself or the other optical elements that the beam encounter in his path (focus and parabolic mirrors). b) normalized transmission for experimentally measured spectra for internal angles up to total internal reflection angle c) colour map simulated absorptivity: increase of the peak value up to critical condition around 30° *then decrease and broadening*

From the above pictures one can note the divergence of the baseline transmission curve towards higher values above one at low energies, this is coming from the fact that the transmission of the highly doped layer actually decreases for energies below 168meV, as evident in the p- and s-polarized transmission spectra. This can be trace back to an increase of reflectivity below the plasma frequency of the electron gas: the phenomena can be understood in analogy with commonly studied bulk metal case, in which the transmission drops totally to zero, on the other hand this is not observed in our results, since the highly doped slab is less than the penetration skin depth. In this optics we can also understand why the baseline is diverging more and more for increasing angle, since effective length of the QW is increasing.

Light emission from Berreman mode into the free space

We can see how for increasing, but still small angles, the resonance peak is getting more and more deep, sign that the absorptivity is increasing at a very fast rate. A critical coupling condition is expected to be reached when the two decay rates equal each other, so the rate at which the plasmon can decay into the electronic bath is the same of the one through which get optically excited. In this condition a perfect adsorption can be expected. Overcoming this threshold the plasmon is expected to become highly reflective, as the radiative path becomes dominant, more favourite respect to the non-radiative one.
The specular reflection was not measured in the experiment, and as a result, the absorptivity cannot be determined
For the signal performed at Brewster angle, for which there is no reflection component, instead yes:

$$\alpha(\theta,\omega)=\frac{\frac{4\omega_0^2}{(\omega_0+\omega)^2}\frac{\gamma_{NR}\Gamma_{rad}(\theta,\omega)}{2}}{(\omega-\omega_0)^2+\frac{4\omega_0^2}{(\omega_0+\omega)^2}\left[\frac{\gamma_{NR}}{2}+\frac{\Gamma_{rad}(\theta,\omega)}{2}\right]^2}$$

For small incidence angles for which is valid the condition of non-radiative decay rate much greater than the radiative one, the expression can be simplified to a Lorentzian with a linewidth characterized by gamma non-radiative only

$$\alpha(\theta,\omega)=\frac{2}{\gamma_{NR}}\frac{2\Gamma_{rad}}{1+\left(\frac{\omega-\omega_0}{\gamma_{NR}/2}\right)^2}$$

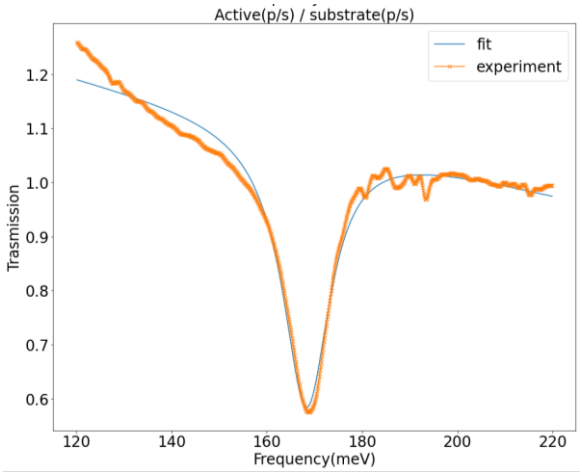

$$A*\left[1-\frac{1}{\frac{\Gamma_{NR}}{2}}\frac{2\Gamma_{rad}}{1+\left(\frac{\omega-\omega_0}{\Gamma_{NR}}\right)^2}\right]+a\omega+C$$

Figure 6 Fitting transmission at Brewster angle and fitting function used taking in consideration also a linear baseline

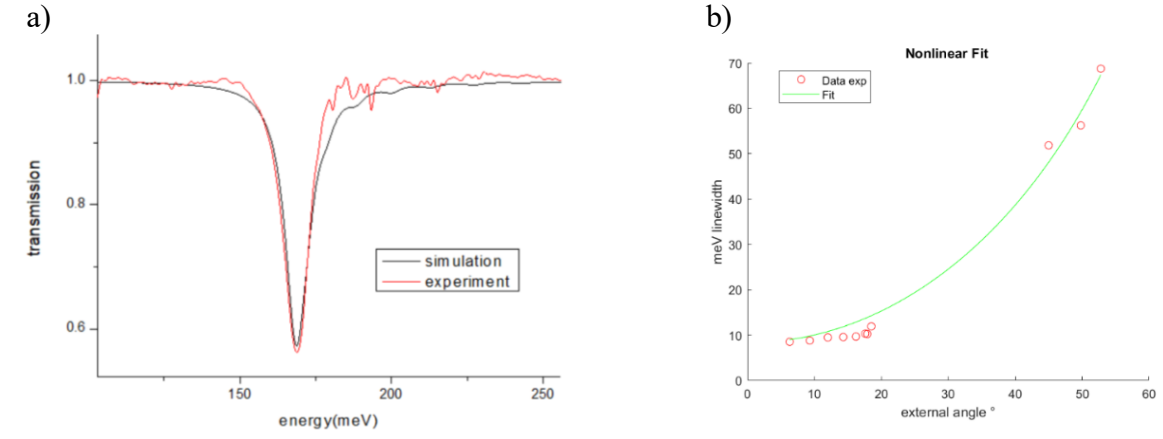

Figure 7 a) overlap of experimentally measured spectra and simulated one for Brewster angle, resonance peak at 168.75meV -> effective doping of $1.89e19\ cm^{-3}$ *, slightly lower than the nominal one of* $2e19\ cm^{-3}$ *b) fitting of the experimental linewidth data with the previous equation* $\Gamma rad(\theta)=N_s\frac{2\alpha}{m^*}\frac{\pi\hbar}{n}\frac{sin\,\theta^2}{cos\,\theta}$ *(1)*

From

The fit, performed on the experimental data following eq. $\Gamma rad(\theta) = N_s \frac{2\alpha}{m^*}\frac{\pi\hbar}{n}\frac{sin\,\theta^2}{cos\,\theta}$ (1), allows us to find the value of the areal electron density Ns, which is in very good agreement with the volume density of $1.89e19\ cm^{-3}$, obtained by matching the peak energy of the simulations and that of the experimental spectra.

It is to be pointed out that the perfectly rectangular well used in the simulation does not correspond to the real potential profile felt by the electrons. Here the quantum well boundaries are not defined by different materials, but indeed the high doping used in the 150nm layer of InGaAs lead to a significant band bending. The real band structure can be obtained quantum mechanically from self-consistent solution of the Schrödinger-Poisson equations with a resulting electronic potential (coming from the balance with diffusion potential) sufficiently strong to localize the electron gas.

Measurement strategy: ATR-FTIR spectroscopy – multipass configuration

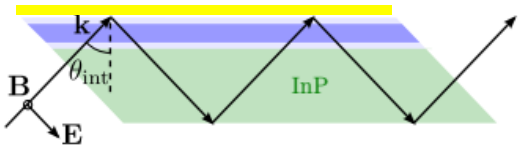

Figure 8 Schematic of multipass from Haki, sample with 45 polished facets

For the second sample of the same type of doping, the beam undergoes multiple internal reflections within the crystal, interacting with the plasmon at each reflection point, increasing so the effective interaction length, this would be in particular favourable in case of very low adsorption signals (similar configuration is used in Attenuated Total internal Reflection), this, as has been highlighted previously is not our case, so a saturation effect is expected. A layer of gold has been deposited on top, in this case, so when the Berreman mode is next to a metallic mirror, a factor of two must be included in the previous general formula for absorptivity. In the first case the transmission measurement can be done up to an internal angle of 18.8, corresponding to a nearly grazing external angle, with this configuration we get the advantage to have the possibility to access to wider angles. Moreover, here can be observed a blue shift effect of the Berremn mode manifestation of the cooperative Lamb shift (G.Frucci, 2017)

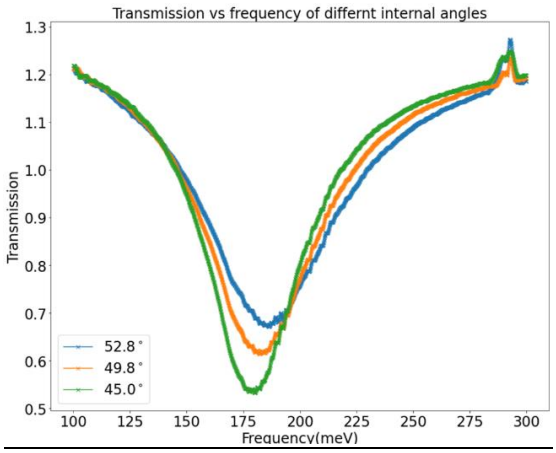

Figure 9 Transmission multipass

I would like to emphasize that the specific architecture here used, effectively is just the same of ATR-FTIR experiments, and is especially intriguing for the upcoming studies that aim to investigate the coupled system water-plasmon (see Figure 31).schematic attenuated total internal reflection experiment with insight of the interface evanescent wave (around 100nm)

Results for 15nm doped layer

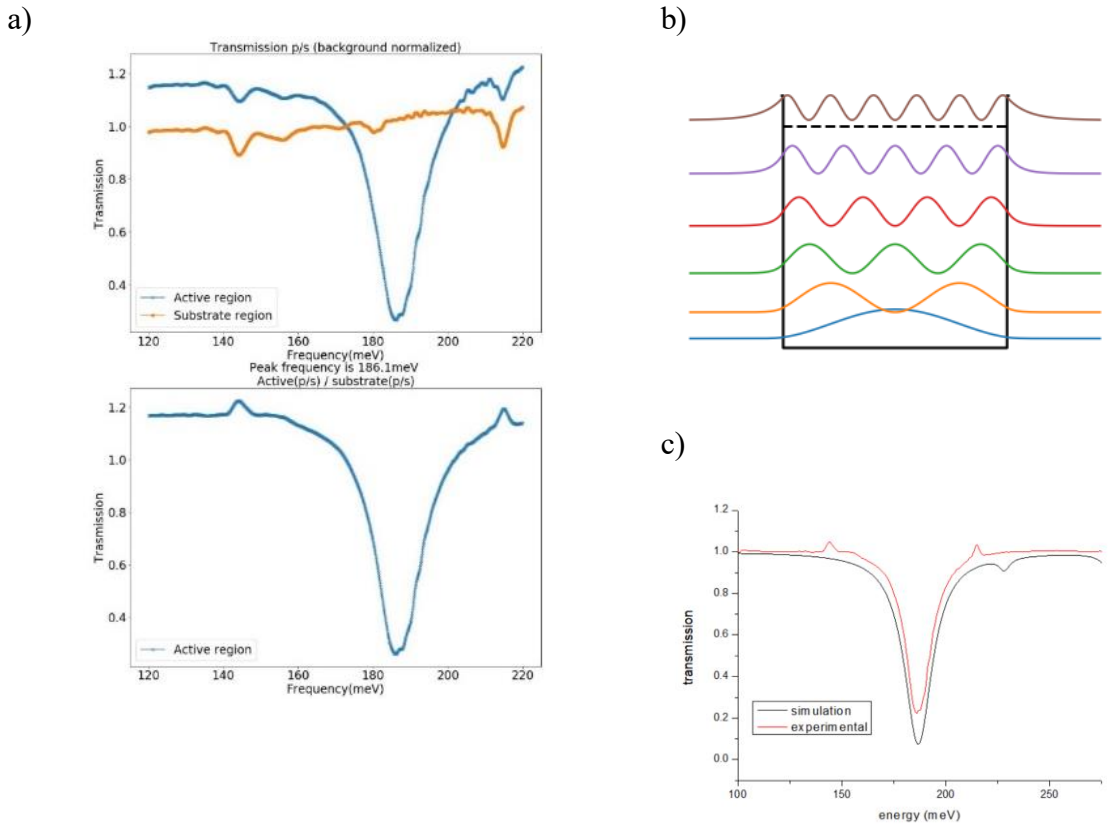

Figure 10 a) Acquisition of the spectra for different substrate and different polarizations b) rectangular potential well model and square moduli of the wavefunctions c) experimental and simulated peak of transmission

The doping level is the same as the precedent sample, but in this case the highly doped layer is just 15nm thick. Both the two samples present a single sharp resonance peak , but the microscopic nature of the system is changed: from 15nm well to the 150nm one, keeping the same doping level so same electronic density, the number of occupied subbands increase a lot and the transition energies get smaller and smaller (see fig 5.a and 11.b) By increasing the quantum well thickness the number of occupied subbands is increased, and so a larger number of transitions get optically excited.

Confinement energy

Worth making the comparison between the measurement done between the two samples having different doping levels: these have same nominal electronic density per unit volume, having be subjected to the same doping process, different resonance energies are expected due to the different electronic confinement. In the 15nm QW case only few electronic subbands are occupied and the resulting plasmon mode will be given by two contributions, one of confinement that is related to the existence of an energy separation between the electronic states induced by the size limitation.

$$E_{Pl} = \sqrt{E_P^2 + E_c^2}$$

where Ep is the bulk plasma energy and Ec the confinement energy that in our case result to be 80.6 meV

We distinguish so two different contributions to the resonance energy, one associated with the electronic confinement and the other with the collective nature of the excitation, seeing in the first one a possible parameter that can be varied to tune the resonance position. Increasing the quantum width and hence the number of occupied subbands, the confinement contribution (coming from inter sub-band plasmon) progressively decreases and become a negligible fraction of the resonance energy. (B.Askenazi, 2014)

Graphene-Liquid interface

General introduction - Graphene

Graphene, a single layer of carbon atoms arranged in a two-dimensional honeycomb lattice, has garnered significant attention since its isolation in 2004 with exotic electronic properties stemming from its unique band structure : being a zero-gap semiconductor (conduction band and valence band touch at the Dirac point) where charge carriers can be ascribed as massless Dirac fermions, having a relativistic linear energy- momentum dispersion. Ideally graphene is a charge neutral material, which can be easily doped electrically or chemically (including surface doping, simple adsorption of molecules without altering the structure). In the electronic device domain in particular Graphene-Field-Effect transistor (GFET) has emerged taking advantage of the exceptional electronic properties of the 2D material as channel in between source and drain contacts, rather than semiconducting material, boasting a room temperature high electron mobility, with significant promises for high frequency electronics, but naturally a lower on-off ratio due to the lack of the band gap, with consequent limits for digital electronic applications (in case of traditional FET the bias voltage enables the current to flow, whereas in absence of this the material acts as an insulator). Still GFET are very promising for analog applications (high speed of switch, good for terahertz) and attractive for the sensing world, since the channel is directly exposed to the environment or material under test (bio and chemical sensing for example, the attaching or detaching of a molecule induce a change in current).
Another advantage in the use of graphene is its geometrical 2D nature with respect to the classical 3D structure of the silicon on insulator technology: there is no body or bulk charge in a purely 2D system, that can degrade the device performance. In recent years moreover the possibility of fabricate large area graphene samples, with good uniformity, has improved, with synthetic growth of films of it though CVD technique on metal substrate like copper.
As in any other FED, the voltage applied through the back gate (capacitively coupled to graphene through the use of dielectric material, recently promising the addiction of hBN to improve mobility) tuns the charge carrier density in the channel: applying a positive of negative voltage, the Fermi energy level is tuned, relatively to the DP, upwards or downwards, resulting so in an electron or hole conduction mechanism (ambipolar effect).
This “intrinsic graphene” with the Fermi level precisely at the Dirac point has no free carriers and is obviously an ideal model, because the slightest amount of doping or external potential perturbation will induce carriers in the system. The real “extrinsic graphene” manifest charged impurity disorder or spatial-topographic inhomogeneities that will render this intrinsic graphene experimentally unrealizable.
Injection of carriers is determined by the electrostatic potential configuration of the graphene environment and, depending on which is larger, could be dominated either by the external gate voltage or by charged impurities.
It has being evidenced by different works that the value of minimum conductivity measured is greatly correlated to charge fluctuations, which can be have been claimed to be caused by different sources as topographical corrugations, charge-donating impurities, surface contaminants like adsorbed molecules, but also metal contacts, all of them of them introducing a certain degree of disorder (acting as Coulomb long-range scattering centre and so causing moreover a limit of electron mobility).

CVD graphene transistor preparation

In particular the raw material was a single/layer graphene grown on a copper foil substrate bought from Graphenea. The layers of graphene were properly transferred on the previously realized platforms (Si/SiO2 substrate with deposited Ti/Au electrodes) using the PMMA-based technique. PMMA diluted in anisole was spin coated on the graphene film, then annealed for few minutes at 80 degrees. In order to etch away the copper foil the graphene/PMMA film was immersed in copper etchant for four hours.
Then to rinse the suspended graphene layer on PMMA the following procedure has been done:

- Progressive deluition of the etchant solution by the use of pipettes, dilution helps to control the etching rate, making the process gentler
- “fishing” the sample (using glass slide cleaned through oxygen plasma exposure) from the etchant solution and then dip it gently into a baker filled with deionized water, let the PMMA/graphene float on the surface for a minute and then repeat three the same procedure with clean deionized water baths, in order to be sure to have removed any copper etchant residual.

The target substrate Si/SiO2 was cleaned using acetone and IPA and then dried using a nitrogen gun. Subsequently, the graphene/PMMA film was scooped out of water bath and transferred onto it, carefully aligning it, by means of the same fishing technique described before for the rising process. Then we let dry the sample in ambient condition under the hood. Then another heating step at 120 degree to help flatten eventual imperfections, ensuring a smoother and more robust film. Indeed the layer of graphene has ben lying not on a perfect flat surface, but on a rough metal one, by consequence there are always some small gaps between the graphene and the target sample, regions in which the graphene is not fully attached and where tends to break easily, or forming cracks. The transfer process, in particular for large area graphene, is improved by introducing a second PMMA coating step (using a more diluited solution): a liquid PMMA solution was dropped to cover the previous cured PMMA layers, thus partially dissolving it, such redissolution tends to mechanically relax the underlying graphene, guaranteeing uniformity and good adhesion. Thanks to this during the consequent dissolution procedure in acetone bath the tension

Final step is to store the sample in an acetone bath for about 4h to dissolve PMMA.

(Despite the care in the whole process wrinkles or tears can be present, the origin of them can be attributed also to a difference in the coefficient of thermal expansion between graphene and Cu substrate, as well as other studies report a possible influence of the crystal domain orientations in Cu. Moreover residual PMMA or etching byproducts can remain on the graphene affecting its properties)

a) b)

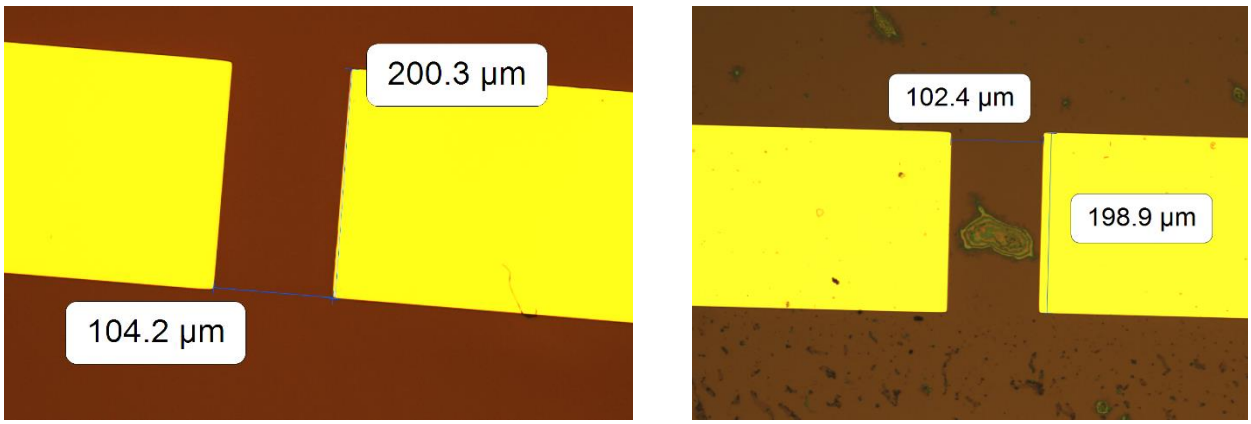

Figure 11 Optical microscope images: a)clear graphene without ripples or PMMA residuals b) clear evidence of presence of ripples and PMMA leftovers

Raman characterization

The production of large are and defect-free monolayer graphene is still challenging, very often domains of defects (wrinkles, impurities, ..) and/or multilayers, compromising the performance of the material. Raman spectroscopy present itself as the best technique, fast and non-destructive, to give a first estimation of the quality of the material.

a) b)

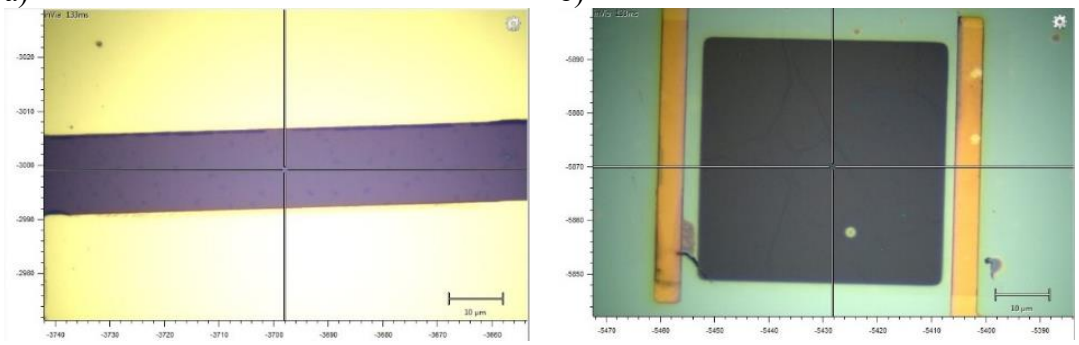

Figure 12 a) home CVD graphene b) commercial GFET S-20 chip from Graphenea (this last samples used for other measurement about ionic liquid doping on graphene here not reported)

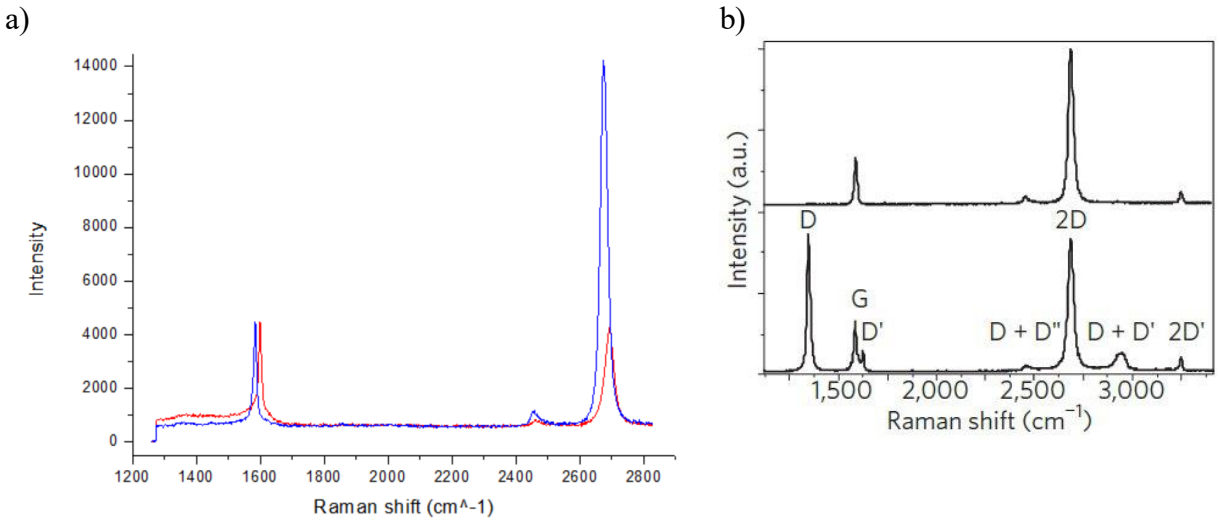

Figure 13 a) In blue the commercial sample Raman response and in red the one of the home-made graphene. b) Raman spectra of pristine (top) and defected (bottom) graphene with main peaks labelled from (M.Basko)

It has been performed a Raman characterization of the CVD graphene used than in the experiment. As can be seen from the data, we have obtained a very typical SLG spectrum with distinct bands.
Three are the main strong peaks that appear in the spectra, and are characteristics indeed of carbon materials exhibiting a sp2 hybridization, usually reported in the literature for graphene analysis:

- G peak around 1580 corresponds to the high frequency E2g phonon at gamma point, centre of Brilluein zone.
- D peak around 1350 correspond to a Raman forbidden mode, not visible in the pristine graphene, since require the presence of defects for its activation (this is due to the breathing mode of six-atoms rings). The defect provide the missing momentum contribution to satisfy the relative Raman selection rule. This peak founds its origin in an intervalley double resonance scattering process at K point. A similar scattering mechanism can also occur at K', producing the so called D' peak, usually less intense than the D one and appearing as a shoulder of the G peak, widening it.
- The 2D peak correspond to the D peak overtone, where in this case the conservation of momentum is ensured by scattering of two phonons with opposite wavevectors , no need of a defect for the second inelastic scattering, for this reason such feature is always present in the Raman spectra of graphene, regardless of the quality of it.

Raman maps

It has been performed a map scanning of different are of the graphene, for each pixel three acquisition were performed to average the result, the Raman peaks were then fitted each with Lorentzian line shape, arising from a finite homogeneous lifetime broadening. Then different 2D maps can be obtained from the acquired data choosing to plot different peak fitting parameters, as the peak height (intensity), peak area, or peak energy position or FWHM.
For example, it is possible to recognize monolayer graphene domains with respect to multilayer regions: the difference in between the band structures of mono layer of multilayer graphene is indeed reflected in the shape of the 2D peak (already over 5 layers the feature becomes no more distinguishable respect to that of graphite), moving from a single sharp peak for the monolayer case to four component in the bilayer case, following the evolution of the electronic band structure and phonon dispersion relations becoming more complex with contribution from more different process becoming possible (as interlayer interactions).

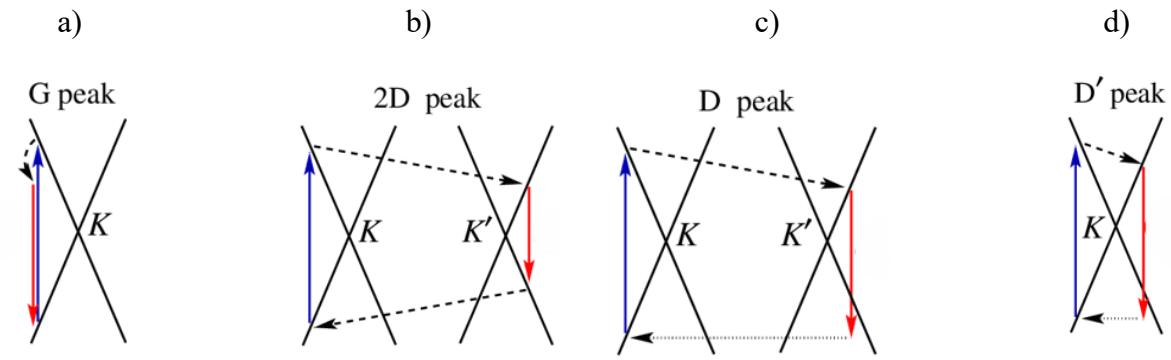

Figura 1 a) intravalley one-phonon G peak b) intervalley two-phonon 2Dpeak c) defect assisted intervalley one-phonon D peak d) defect assisted intravalley one-phonon peak. Blue arrow for the adsorbed photon, red arrow for the emitted photon, dashed arrows for phonon emission and electron scattering from a defect represented by horizontal dotted

The objective of the analysis was in particular to get an estimation of the amount of defects present in our samples and their dimension, with the name "defects" meaning everything that breaks the hexagonal symmetry in graphene, can be because of chemical adsorbates or structural modifications.

Generally to study their amount it is considered the integrated intensity ratio of the D to G peaks (ID/IG ratio) indeed the enhancement of it is usually related to an increase of defect density (care must be taken in distinguish when is used the intensity, peak heigh, or integrated intensity, peak area). The relation in between these two is however limited to Raman active defects, charged impurities are not be said to degenerate the D peak. For this types of defects other Raman features are used, 2D and G peaks are more influenced and more useful for later discussion. (C.Casiraghi, 2007)

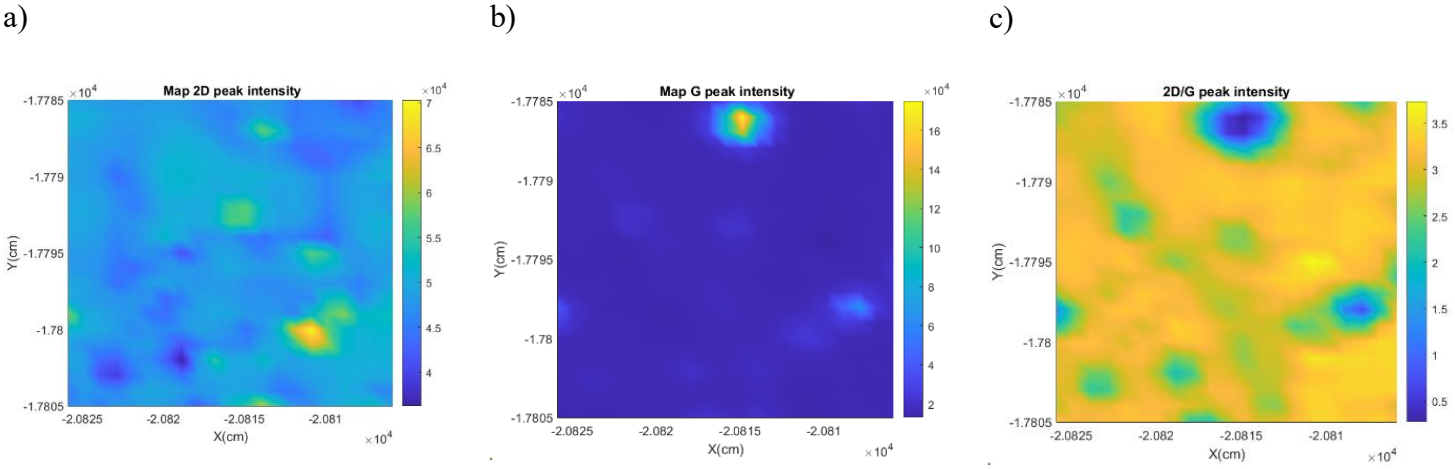

Figure 14 Raman maps of a) 2D peak intensity, b) G peak intensity, c) 2D/G ratio of intensities (532nm laser)

Previous work - moving droplet capacitance

We introduce now the set up specifically designed to probe the interaction of graphene transistor with micrometric droplet flows. The primary objective of the experiment was to study possible liquid flow-induced currents in the 2D material based transistor. Preliminary results, with a similar experimental idea, were already obtained: an example is the study of (Guo, 2014) in which it has been observed how a salted droplet moved on top of graphene is inducing in it a "drawing potential". In correspondence of the liquid spot there is the formation of an electrical double layer realized by the adsorbed ions and the induced accumulation of a layer of opposite charges in graphene, this can be picture as a pseudo- capacitance (Debye double layer) that when is making advance will drag electrons in graphene (charging and discharging at the boundary of the droplet, inducing an higher potential at the front than at the tail). Other works about the coupling between ion and electron dynamics are (S.Ghosh, 2003) and (Rabinowitz, 2020). Overall many studies have been carried out in the scenario of ionic Coloumb drag.

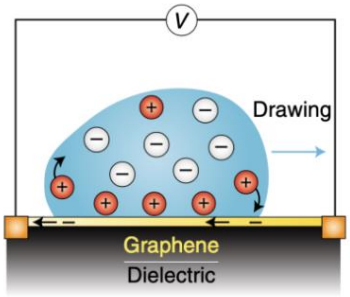

Figure 15 electricty generation moving a droplet on CVD graphene. Charges are adsorbed at the advancing contact line and desorbed at the receding one (Guo, 2014)

Measurement strategy and home made set up

The strategy of study is to really look at the fundamental interlayer coupling mechanisms taking advantage of single microdroplet on high quality graphene. A small amount of the solution is deposited and moved over the graphene transistor while monitoring the drain source current, applying a bias of 100mV.

The tuning fork atomic force microscope (AFM) homemade set up allows for a precise control of the distance between the prone and the samples surface, necessary in our case to avoid scratching of graphene. It is applied a frequency modulation technique using a macroscopic aluminium resonator. This is excited at its resonance frequency f_0 (approximately 1.2 kHz) in the normal mode using a piezo-dither. The amplitude and phase shift of the tuning fork oscillations are measured via an accelerometer glued at the end of the prong.

Our custom-built AFM operates in frequency-modulation mode, utilizing a Phase Lock Loop (PLL) to ensure the tuning fork is consistently excited at its resonant frequency. Additionally, a Proportional Integral Derivative (PID) servo loop maintains a constant oscillation amplitude by adjusting the excitation voltage. Interactions with the substrate are detected through changes in the resonance frequency and excitation voltage

Pipette

Use of a Sutter Instrument P-200 pipette puller to obtain the capillary tip (by tuning the pulling parameters different diameters and geometries can be obtained)

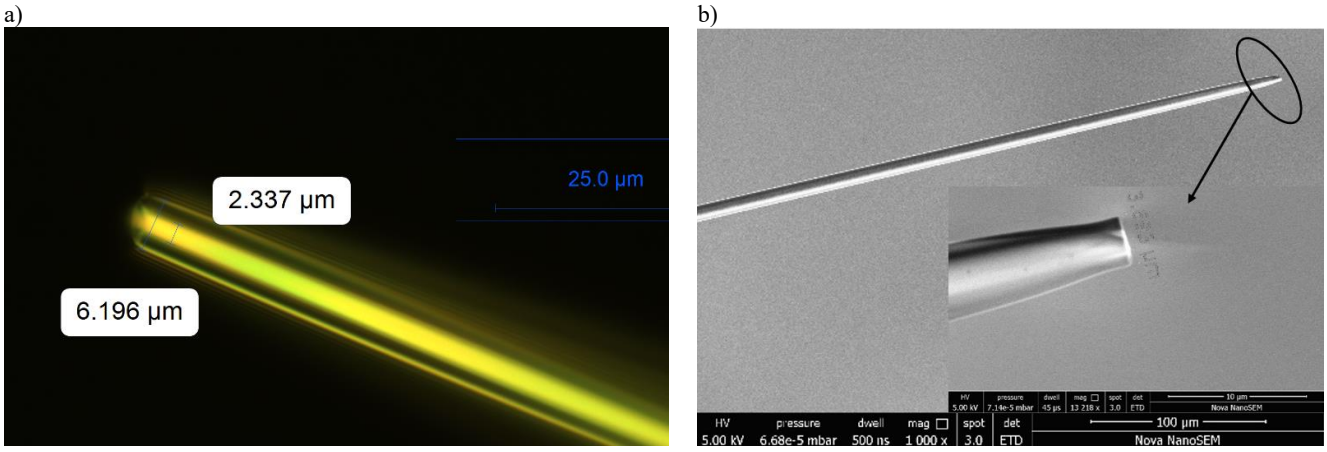

Figure 16 a)optical microscopy image and b) Scanning Electron Microscopy image of pipettes used

AFM set up

In our experiment we make use of an Atomic Force Microscope, in few words we remind how this is one currently one of the scanning probe technique with the highest resolution, limited just by the curvature of the sharp tip, that can be easily nanometric, mounted on a flexible cantilever. Commonly this is used to obtain topographic images of different samples: the interaction forces in between the probe and the surface are measured, the increase of them when the tip is closer to material induce a change in the motion of the cantilever, this is detected and used in a retro-action loop to impose a constant interaction force and so a constant distance in between the tip and surface.

In the standard set up (all) used in particular as a force sensor is used a centimetric tuning force like the one represented in the upper image. The fork geometry is quite versatile allowing for easily mounting a wide selection of tips, and in our case pipettes. In order to dynamically control the normal and shear oscillation, a piezo dither can excite both oscillation modes of the tuning fork, indeed the prongs of the tuning fork can oscillate along a shear and a normal mode simultaneously. A two-axis accelerometer can be used to monitor the resulting amplitudes of both the two and also phase difference between excitation and oscillation signals (dynamic oscillation amplitude).
For each oscillation mode a PLL tracks the resonance frequency (ω) and a PID retroactively adjust the intensity of the excitation input (F) to keep the oscillation amplitude constant. The electronic control is performed with a Nanonis controller which possesses its own data treatment software and force spectroscopy module
In principle many resonance frequencies are possible for this system corresponding to different modes of oscillations, in the following we always make use of the resonance corresponding to a normal displacement of the prongs (with the first order mode of the normal oscillation characterized by a resonance frequency around 1KHz, tangential resonance frequency is expected a lower values).

Reversed AFM set up

Before starting the experiments, the set up has been revisited in a "reversed-configuration" that allows to operate the measurement in an easier and faster way: the 'active part' is no more the one of the probe, the tuning fork is no more the component put in oscillation, but the cantilever on which the sample is mounted on, in particular an aluminium resonator which is putted in oscillation by means of a piezo-dither and whose frequencies of movement are measured by an accelerometer. Again, for the beam exist many resonance modes, and the accelerometer is able to monitor both x and y oscillation modes, but for our purposes we will monitor just the normal modes. The pipette is placed on the head of a 3-axis piezo-scanner using a double sided tape (no more difficult mounting on a millimetric tuning fork).
In the following measurement we will always operate the instrument in frequency-modulation mode, exciting the resonator via a piezo-dither at its resonant frequency in the normal mode, measuring in real time parameters like the shift from resonance frequency, the amplitude at this one and the excitation voltage that is necessary to provide to maintain the amplitude of oscillation constant.

Lock-in measurement (Specs Nanonis package)

A lock-in amplifier system is used to extract the amplitude of oscillation and the phase shift of this one with respect to the excitation voltage at excitation frequency. Generally speaking the lock-in measurement are suited to acquire very small AC signals, that in many cases can be obscured by noise. In particular are used two-phase lock-in amplifier: implementation of a second detector, that performs the same computation but with an additional $\pi/2$ phase-shift, in this way we obtain not only the voltage response amplitude, but also the phase shift of input signal with respect to reference one.

PLL

To systematically excite the beam at its resonance and to measure the shift in this frequency induced by the interaction forces in between probe and sample, is used a Phase Lock Loop (PLL): the phase shift extracted from the lock-in is compared to a reference phase shift of $\pi/2$, then a voltage controller oscillator generates a signal that is injected into the piezo-dither, which will be the new reference signal for the lock-in through a feedback loop, to ensure a constant phase shift between the excitation signal and the resonator oscillation. In this mechanism is a PID (proportional-integral-derivative controller) that acts as a control loop with a negative retroaction, this allows to measure what is the necessary variation in the excitation voltage necessary to maintain constant the oscillation amplitude.

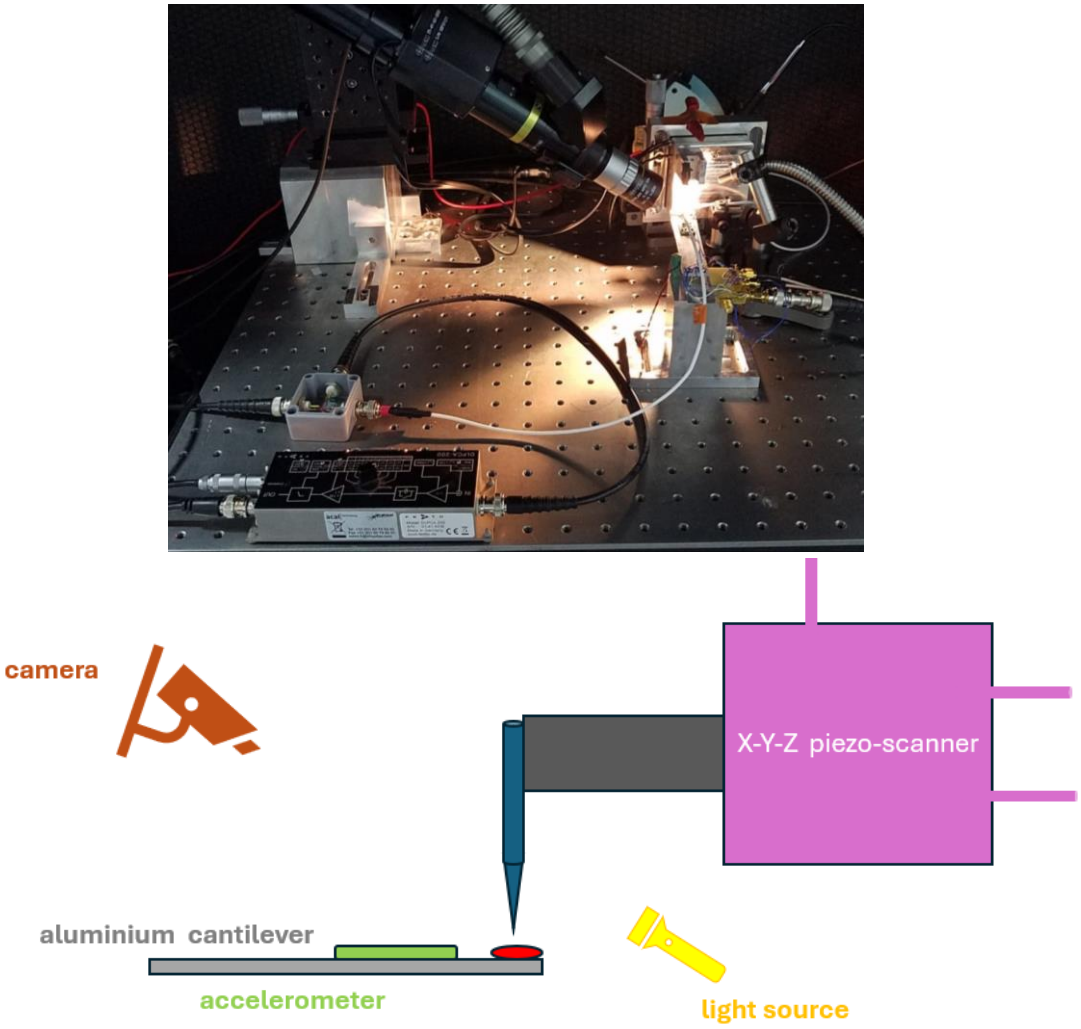

Figure 17 photo of the experimental set up and schematic of it. 3D scanner for a manual coarse approach of the pipette to the sample and a piezo scanner for fine final one with sub nanometric resolution

All the precautions mentioned above are meant to allow the creation in a fast way of a micrometric droplet without damaging the graphene.

Droplet formation and control

Two modules provided by the Specs Nanonis package allow for the precise positioning of the tip on the sample: the Z-controller and the Scan Control module.

The Scan Control module allows for the adjustment of the pipette's tip's lateral position above the sample and facilitates the scanning of the sample for imaging maps. This module enables the selection of the imaged area's size, the scanning speed of the tip, and the scanning axis angle relative to the x and y axes. After the tip is manually positioned above the sample in the desired position between the electrodes and the tip-sample distance is within the range of the xyz piezo-scanner, the Z-controller can be activated to gently approach the tip to the substrate. The PLL control detects the moment of contact, and in our case, the formation of a droplet, which causes a sharp shift in resonance frequency, indicating increased contact stiffness. The pipette is then slightly retracted, measuring a relaxation in the frequency shift signal until an equilibrium set-point is reached, where a hydrostatic equilibrium forms between the liquid in the pipette and the droplet, resulting in a liquid capillary bridge. The lateral size of the deposited droplets depends mainly on the pipette's outer diameter and the substrate's wetting properties (spread of the droplet with a low contact angle). Through the Scanner Control window, the pipette can be moved along the XY-plane with the droplet that remains attached to the tip and be slid across the surface.

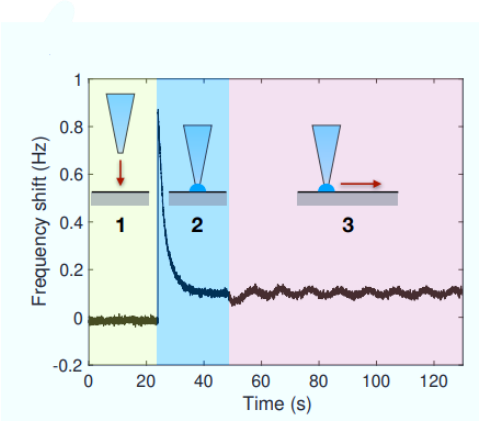

Figure 18 Monitoring of the frequency shift response of the AFM during the final approach. Initially, the pipette makes contact with the sample (1). Following contact, a slow relaxation phase (2) indicates droplet formation. Image from (Marcotte, 2021) deposition and movement of the droplet in such case realized through the use of a quartz tuning fork used before for previous experiments

Installation of the sample in the set up

The sample is cleaved with a diamond tip from the wafer. This is then fixed by means of a stripe of carbon tape gently on a few centimetres long copper plate, along with two centimetric gold coated aluminium oxide pads. The two Ti/Au electrodes on the sample are then connected to the packaging by wire bonding. The device so can be integrated into the whole experimental set-up by simple soldering of copper wires on the gold pads.

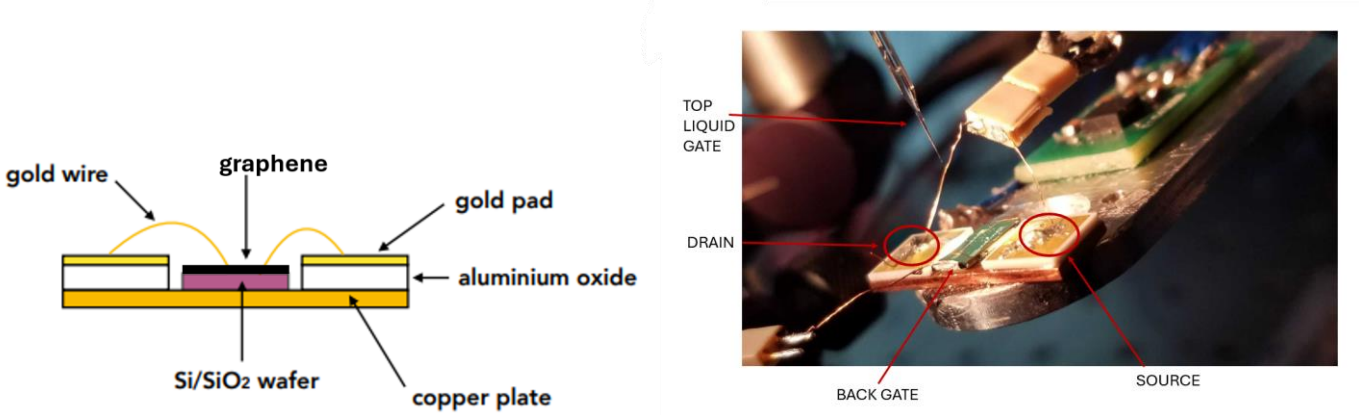

Figure 19 Schematic of how the sample has been integrated on a chip for electrical measuraments and zoom in the set-up experiment

Top EDL-gating principle

The idea comes from EDL transistor, which are field effect transistor where the solid gate dielectric is replaced by a ionic liquid, with an enhancement of the channel/gate coupling of more than one order of magnitude, thanks to the formation of outstanding capacitance. Through the use of this gating technique, high charge carrier densities can be induced in the channel of the transistor as never been reached before.

Looking at the schematic figures can be understood that when no voltages is applied the ions are randomly mixed guaranteeing a charge neutrality condition. When instead a positive gate voltage is applied the ions will rearrange themselves according to the potential gradient induced: ions of same polarity of the top electrode are going to be repulsed from this latter one and accumulate at the channel interface. The charged layer that is here so formed is compensated by the injection of charges of opposite sign in the conducting material.

Obviously applying a negative gate voltage the situation is just reversed, with the formation of a p-type channel. We can model the capacitance that is formed at the interface like a parallel plate capacitor with a sub-nanometric dielectric thickness, leading to exceptional large geometrical areal capacitance (around $10uF/cm^{-2}$)The potential applied between the gate electrode inside the liquid and the sample falls predominantly over the atomically thin EDL, thanks to this it can be overcome an important problem of solid-state FETs: in this standard devices the maximum achievable carrier density is limited by the breakdown of the gate dielectrics, happening around 1V/nm for already the ones having the largest

strength, in the liquid gating the only limitation comes from electrochemical degeneration of the material or electrodes (electrochemical window), for this reason the ionic gating enable previously impossible carrier densities

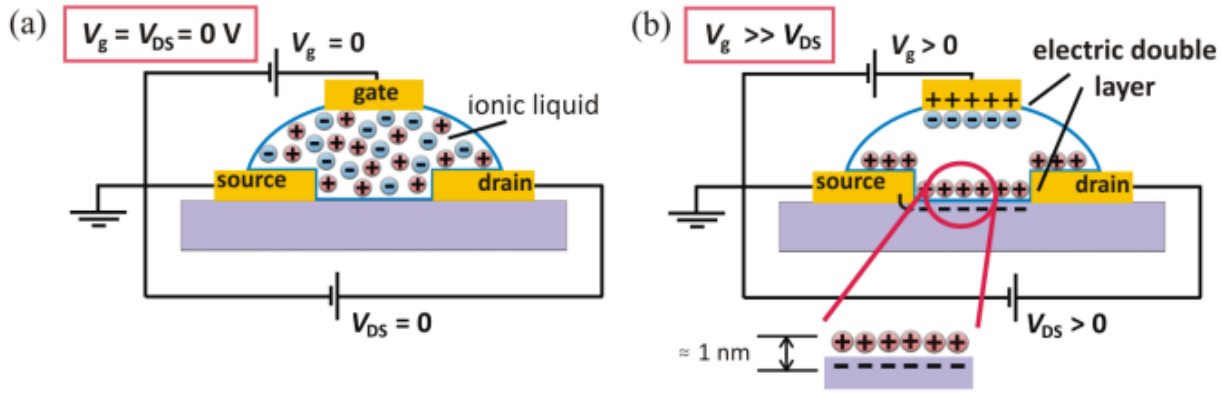

Figure 20 Schematic drawing of an EDL-gated substrate a) without any voltage applied and b)with positive drain-source and gate voltage $V_g \gg V_{ds}$ .. The gate bias leads to the formation of two electric double layers, one at the channel interface and the other at the top liquid gate (J.Seidemann, 2017)

Double gating

In the set up that we are using we could apply both a back gate and also a top liquid gate. This latter in a transistor can be applied by either a metallic wire dipped in a liquid droplet covering the conducting channel or by a counter electrode placed beside the device. In our case we are using a copper wire inserted in the pipette filled by the liquid. Having two gates allow us to explore the effects of an external electric field penetrating a material: the field strength is controlled by the potential difference between the bottom and top gates, while the Fermi level is determined by their sum.

more in appendix about principle of working

Preliminary results

We first discuss the case of the simplest configuration with just a back gate used. The first objective of the experiment was to search for a possible droplet induced current at zero bias voltage: the proposed mechanism (B. Coquinot) for current generation is a phonon-drag-based one.

No bias case

In light of the aim to demonstrate a possible friction- current generation mechanism first measurement were taken moving the droplet without applying any bias in between the electrodes. From the model introduced at the beginning a current in phase with the droplet's velocity. In the measurement taken was observed instead a relation with the droplet's position, shifted by $\pi/2$ with respect to the velocity. The theoretical picture presented before continue to be exquisitely convincing, but maybe not adherent to the following experiment implementation: the phenomenology seems to account for such kind of origin of the current, but the current's phase casts doubts, and the overall mechanism continue to appear as a mystery.

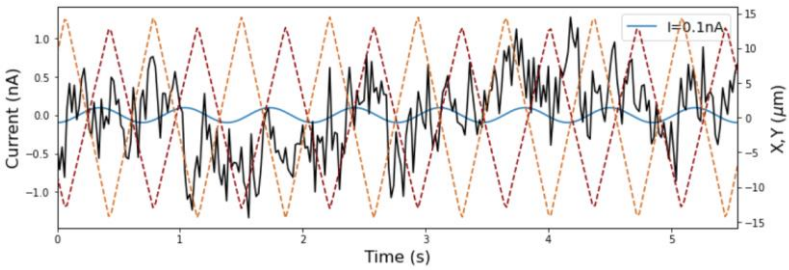

Figure 21 no evident correlation between the movement of droplet and current measured

Applying bias – current modulation

The graphene sample is biased imposing a small voltage drop in between source and drain of 100mV with the liquid droplet put in oscillation. Previously experiments have been performed using transistor realized with exfoliated graphene

and using 5um glycerol droplet. What is observed is a modulation of the drain-source current in phase with the oscillating sliding droplet motion.

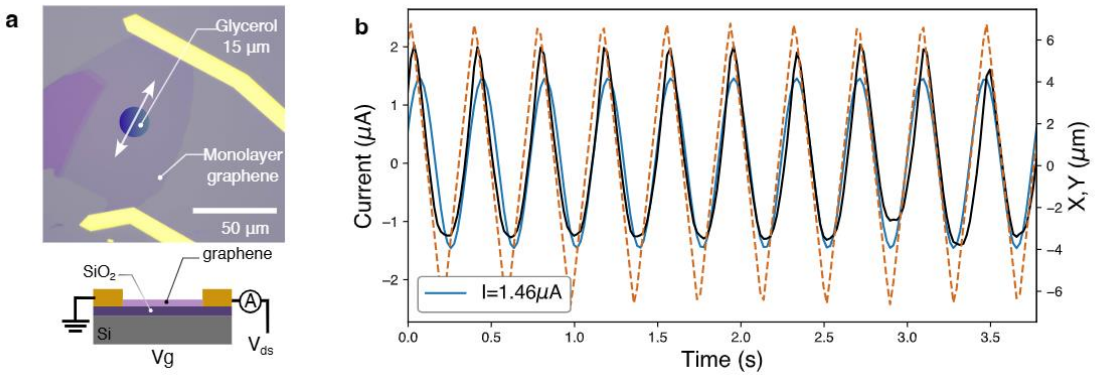

Figure 22 From (Lizee, 2024) he orange dashed line denotes the droplet's position, the black solid line is the recorded current. Blue line is a sinusoidal fit of the current trace

Different liquids have been experienced like room temperature ionic liquid (BMIM-PF6), glycerol, and neutral and apolar silicon oil, with different viscosities but all of them having very small vapour pressures with a nearly zero evaporation (not a negligible aspect considering the small amount of liquid it is used).

Measures

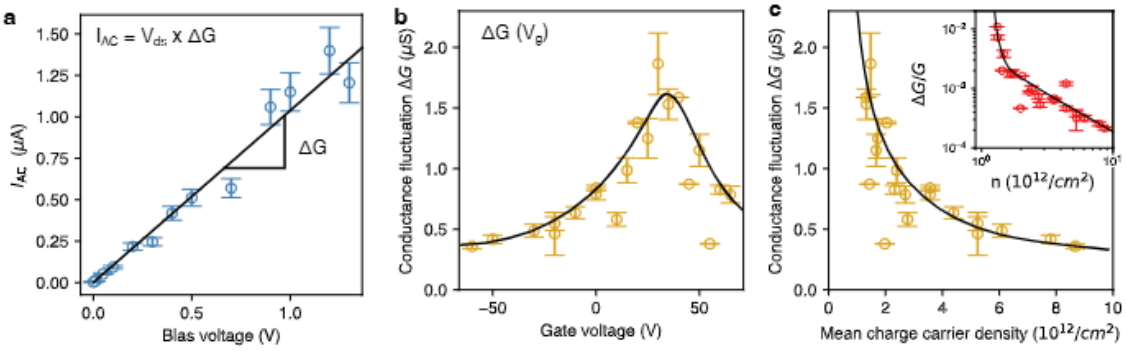

Figure 23 Current and conductance fluctuations versus bias and gate voltage respectively. Same data plotted as a function of charge density (Lizee, 2024)

In the first (a) image can be seen a plot of current's amplitude I_{AC} as a function of the static bias voltage ΔV for a fixed droplet's position and amplitude: a linear proportionality between AC current's amplitude at the droplet's motion frequency and bias voltage arise.

Interpretations

Apparently, the droplet locally modulates the sample's conductance. To rationalize the measurements, we therefore propose the following minimalistic model: the sample's conductance G is a function of the droplet's position $G(x)$(x is a 2d vector). When moving the droplet, the current writes $I(x) = \Delta V G(x, y)$). Considering the linear dependency of current amplitude I_{AC} on oscillation amplitude a, we suppose that the latter is smaller than the scale of the spatial fluctuations of G. We estimate the AC current amplitude to simply write $I_{AC}(x) = a\Delta G(X)$). It can be so formulated the hypothesis that the local conductance gradients that we are seeing can be put in analogy with the ones of STM measurement, where one probes the local differential conductance. (Lizee, 2024)

To have a deeper view of this interpretation, it has been measured the oscillating current as a function of the back-gate voltage. As can be seen from the graphs, the interesting detail is that the amplitude of the conductance fluctuations, obtained just by scanning along a line, is maximum in correspondence of the Dirac peak, where indeed the sample conductance is minimum, and overall all the regions of graphene are, electronically speaking, near the Dirac point. What appears so is that the fluctuations in charge density are enhanced as the mean charge carrier density drops or, in other words, that the conductance's susceptibility to the droplet position is greatly enhanced close to the Dirac peak. The inset

on the upper images sees the normalized conductance fluctuations as a function of the charge density showing a puzzling two-decades increase when the Dirac point is approached.
A possible explanation of such a picture is the one of charged puddles induced fluctuations in the local Fermi level, already measured by means of different techniques such as STM. (S. Samaddar, 2016) and SET (J.Martin, 2007), but also intrinsic ripples can induce local doping in graphene. The droplet moving on the surface of the sample is modifying its dielectric environment and the local charge carrier density tuning the measured conductance

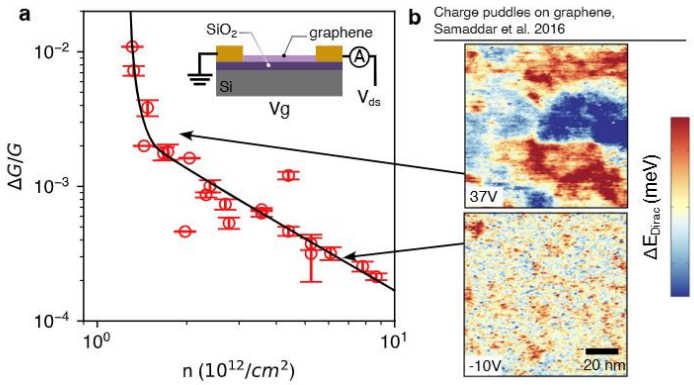

Figure 24 On the right spatial maps of the variations of the local Dirac point energy ED around its spatially averaged value ED, over an area of 100 × 100 nm2 at different gate voltages (S. Samaddar, 2016) Fluctuations in the Dirac point across the sample can be converted into variations of carrier densities, considering that these ones are averaged over an area determined by the tip size.

Imaging charge puddles

Following the experimental findings of (S. Samaddar, 2016), evidencing how both amplitude and spatial extent of the puddles significantly increase as the Fermi level approaches the Dirac point, we have tried to move further correlating the transport measurement with spatial position.
A Vds of 100mV can be applied while scanning the tip over the sample and measuring current in function of tip position, to produce SGM images.

a) 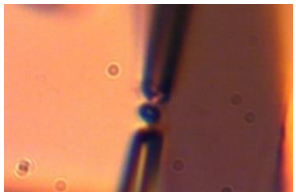 b) 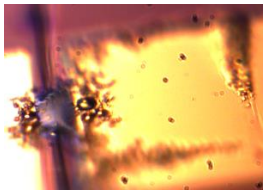

Figure 25 a) fine monitoring of the formation of the droplet through the camera installed near the AFM. Liquid use is a mixture of KCl 300mML and water b) electrochemical effect at 1V

Using very flexible pipette and caring about a gentle approach and contact with the surface are important to not scratch the graphene. Standard back-gated field effect transistor typically always show a positive shift of the Dirac point indicating the presence of a extrinsic hole doping. The samples indeed have been prepared in ambient conditions is so highly probable that molecules from air (such as H2O and N2) trapped between graphene and SiO2 substrate are one likely origin of doping.

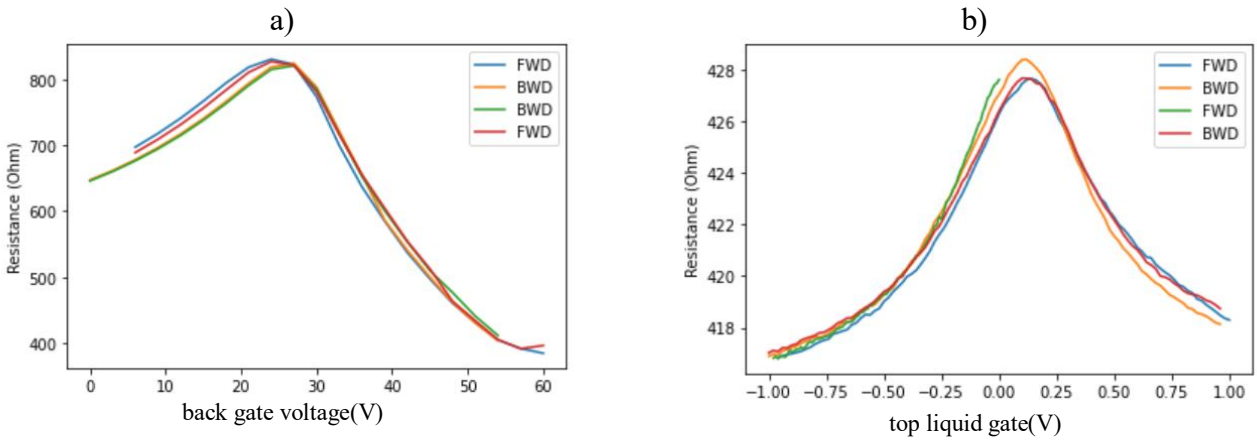

Figure 26 a) back gate voltage sweep b)top liquid gate sweep in both cases clear evidence of Dirac peak evidencing p-doping. BWD, backward direction and FWD, forward direction of sweeping, no hysteresis present, signature of very clean graphene that we have managed to obtain

Post process treatment of the data

For treating the data of the scanning obtained we are using the software Gwyddion implementing a correction for the various artefact that in SPM data can emerge from a line by line acquisition and so facilitating a better visualization of the data and relevant features, always keeping in mind that scan line alignment and correction methods frequently involve heavy data modification which should be avoided if possible.

In particular we have applied: three-point levelling and alignment of rows by median of differences. The first allows to mark three points in the image that should have same values and then a plane is computed from these and subtracted from the data.

Profiles that are taken along the scanning axes can be mutually shifted by some amount or have slightly different slopes. The use of the alignment rows tool allows a correction for this, in particular it has been chosen median of difference, which shift each line so that the median of the value differences (between vertical neighbour pixels) becomes zero. In this way we are ensuring that significant features of the surface are preserved while correcting for inconsistencies, thereby maintaining the integrity of the data.

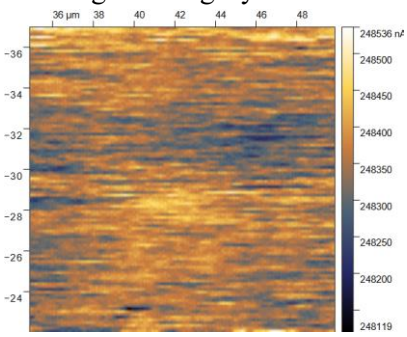

Top liquid gate -1V
Current modulation: 417nA

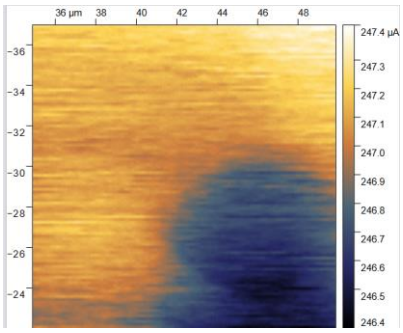

Top liquid gate 260mV
Current modulation: 1100nA

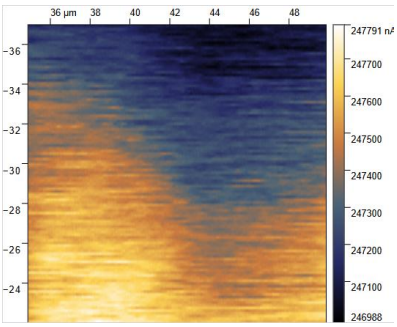

Top liquid gate 750mV
Current modulation: 803nA

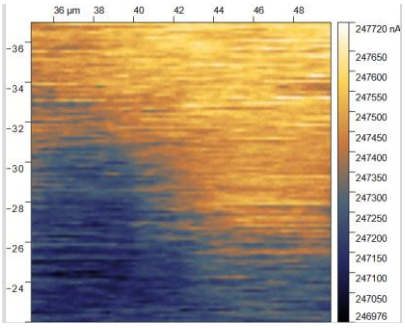

Top liquid gate 0V
Current modulation: 744nA

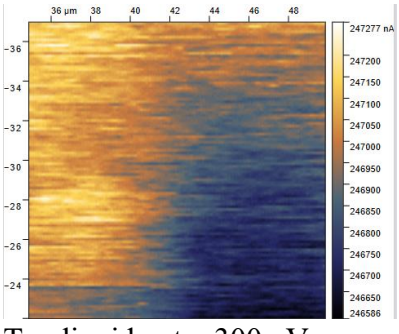

Top liquid gate: 300mV
Current modulation: 691

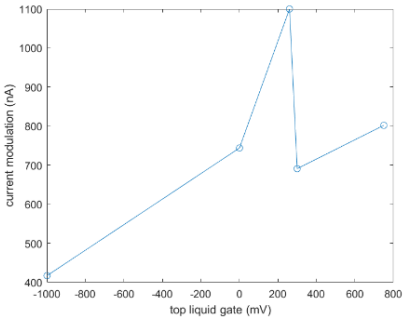

Figure 27 maps of the same graphene area changing top liquid gate bias and observation of different current modulation, evident increase of the magnitude of modulation as the Dirac peak is approached

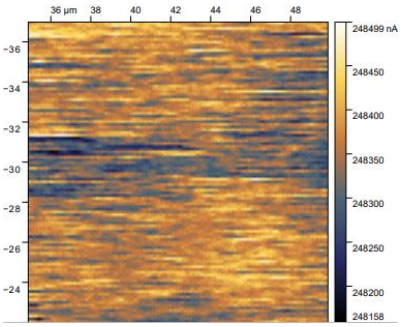

Top liquid gate -1V
Current modulation: 341nA

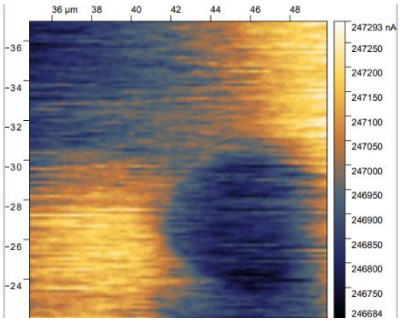

Top liquid gate 260mV
Current modulation: 609nA

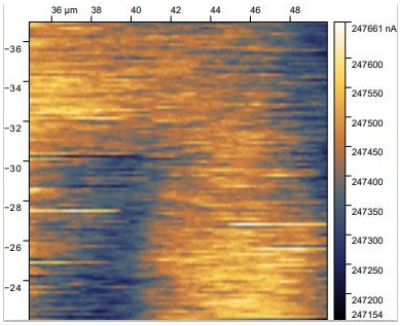

Top liquid gate 750mV
Current modulation: 506nA

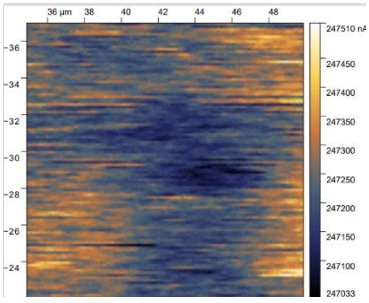

Top liquid gate 0V
Current modulation: 477nA

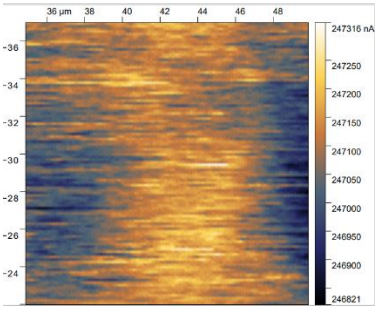

Top liquid gate: 300mV
Current modulation: 495

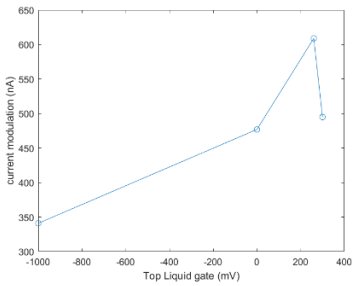

Figure 28 another graphene area scanned, demonstration that the trend before evidenced is reproducible

Interpretation of the acquired maps

Here we have studied how the supposed "charge puddles" develop with the top gate voltage, fixing the back gate at zero. In the acquired maps the top gate voltage spans from -1V up to 750mV (at 1V we have observed water splitting effects, limit of electrochemistry window). What is observed is that interestingly the modulation of currents seems to be with opposite polarity at 750mV with respect to what happen around the Dirac point, 260mV. In other words a switch of the regions with enhanced and depressed resistance, changing the voltage.

Another detail, similar to what observed by (S. Samaddar, 2016) is that both the amplitude and the spatial extend of the puddles significantly increase as the Fermi level approaches the Dirac point. A simple intuition can be proposed to explain how the dimension of the puddles vary with the gate voltage. We can surely assert that in the sample used in the experiment is valid a diffusive regime of transport, being the diffusive length much smaller than the sample dimension. Indeed the diffusive length scales like $1/\sqrt{EF} \sim \sqrt{n}$ so diverging in correspondence of the Dirac peak, confirming so the increase of the charge puddle size (becoming so comparable with our probe limit and so resolvable). The impurity screening is reduced as the charge density decreases, that is approaching the charge neutrality point.

When the Fermi level matches the Dirac peak, the heterogeneity of the impurity charge distribution is the only source of charge carriers (residual density) yielding a much larger screening length which can be accounted for in a self-consistent theory.

In our case we are spatially limited by the dimension of the droplet, so a picture like the one of the reference at -1V would appear like all blurred considering the envelope with our probe. In particular in this work the author has combined the STM with transport measurement to map the Dirac peak as function of the gate voltage.

The pattern (and the magnitude of the spatial variation of resistance response to the tip location) is seen to become subdued and almost disappear when the tip voltage is reduced at -1V, while the features are seen to appear around the Dirac point voltage. We can so say to sum up, that with our measurement we have provided another demonstration of the growth of charge inhomogeneities in graphene near the Dirac point.

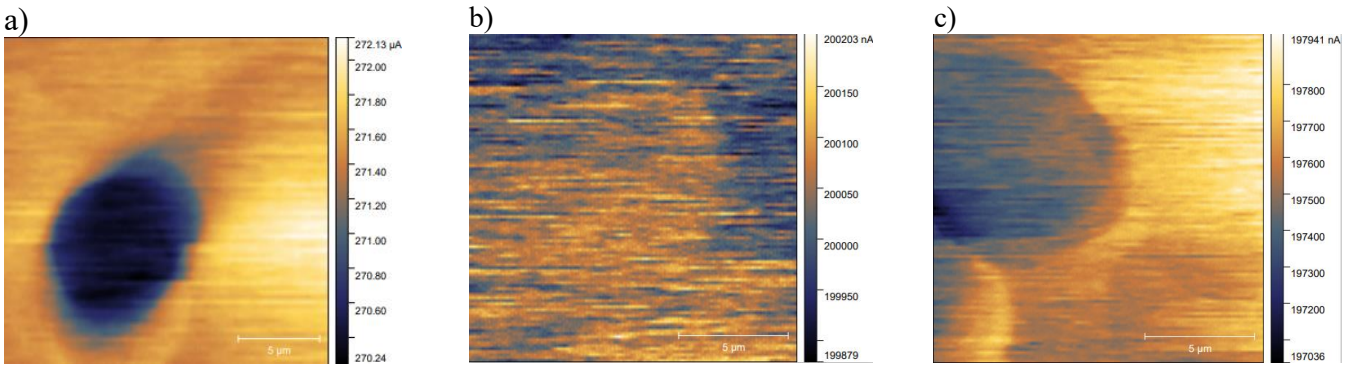

Figure 29 a) high contrast feature, the circular shape coming from the envelop between droplet and the region having different charge density, we can note how the dimension of the feature we have obtained are comparable with the Raman's one b)different area, top liquid gate -1V c) top liquid gate 260mV appearance of defined features

A biased probe, like the one that we are using, can capacitively induce or deplete charge carriers in graphene. The main features of our observations can be understood simply by considering how the electronic transport of graphene with an inhomogeneous carrier density can be affected by local modulation of charge carriers due to the biased probe, which would deplete charge carriers (or equivalently can be thought as inducing charges with opposite polarity) in the graphene underneath.

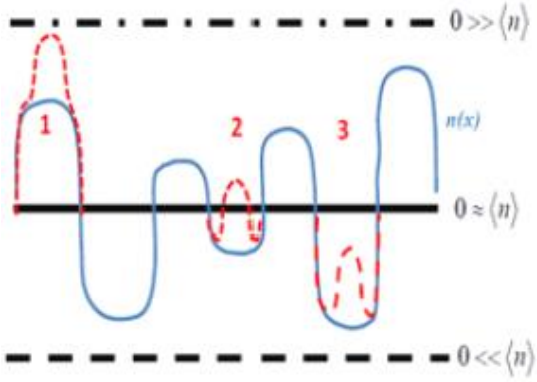

Figure 29 A schematic example of spatially inhomogeneous charge density n(x) (thin blue solid line) and the change (thin red dashed line) due to a negatively biased SGM tip at three representative locations (labeled 1, 2 and 3). The thick black solid line, dot-dashed line and dashed line indicate the zero charge density level for three situations: charge-neutral (<n> ~ 0, with Vbg ~ VD), n-type (<n> << 0, with Vbg > VD), and p-type (<n> >> 0, with Vbg < VD) doping, respectively. This picture from by (Jalilian, 2011)

In the upper figure it is schematically depicted an intrinsic spatially fluctuating carrier density along a line, excluding the induced charges. With the red dotted lines it is instead represented how a negative biased droplet can induce a variation in this one.

When graphene is globally p-type (Vbg << Vdp and $n > 0$, with the thick dashed black line representing the zero carrier density level), a tip with Vtg < 0 would decrease the graphene resistance (R) by adding charge carriers to the sample, whereas a tip with moderate Vtg > 0 would increase R by depleting charge carriers.

We expect the reverse to be true when the graphene is n-type (Vbg>>Vdp and $n < 0$, marked by the thick dashed line).

When instead the graphene is near its global neutral point, so when we are applying a back gate voltage comparable to the one of the Dirac point, the average carrier density is close to zero, as already underlined by previous works, some regions of the substrate are expected to be p-doped and others n-doped, also addressed with the names hole puddles and electrons puddles.

Depending on the position of the tip, the conductance measured will be different, depending on the local properties of the material.

Whatever is the doping type of the region intuitively from the schematic that is shown above we understand that the more the liquid top gate is inducing a change of the carrier density such to move the profile closer to the charge neutrality condition the more the resistance is increased, the more fare away is from the neutrality condition the less is the resistance. In particular, following the reasoning presented above we can assert that when the tip is located above a p-doped spot, applying a negative potential a decrease of resistance is expected like in the (1) case in the scheme, on the contrary the same negatively biased probe on an hole puddle is inducing an increase of resistance (3). Just the opposite complementary result is expected when applying the opposite polarity. Following this argument the nature of charge puddles could be determined observing how the resistance is modulated changing the polarity of the top liquid gate.

Re-interpretation

From such description here we propose a very similar yet slightly different schematic interpretation, starting from the consideration that our sample appear to be generally p-doped, so when applying zero back gate the modulation of charges are not respect to an average zero charge level.
In the underline schematic in green is depicted the "standard case", the modulation of charge carrier density that we can suppose is present in our sample, with one electron puddle and a hole puddle, being the sample generally p-doped the profile is shifted upwards respect to the neutral point. One possible explanation of the results seeing is that when applying a top gate close to the Dirac voltage while scanning, the carriers get depleted: the left n-doped puddle that was before an area of higher resistance now become an area of low resistance, while the right one, that was an area of lower resistance, still remain of low resistance. Applying a voltage higher than the one characteristic of the Dirac point, the picture is inverted: the n-doped puddle now is the area of attenuated resistance, while the p-doped one, on the right, is the one of enhanced resistance (note that the voltages value reported in the schematic are the same used in the maps acquisitions).

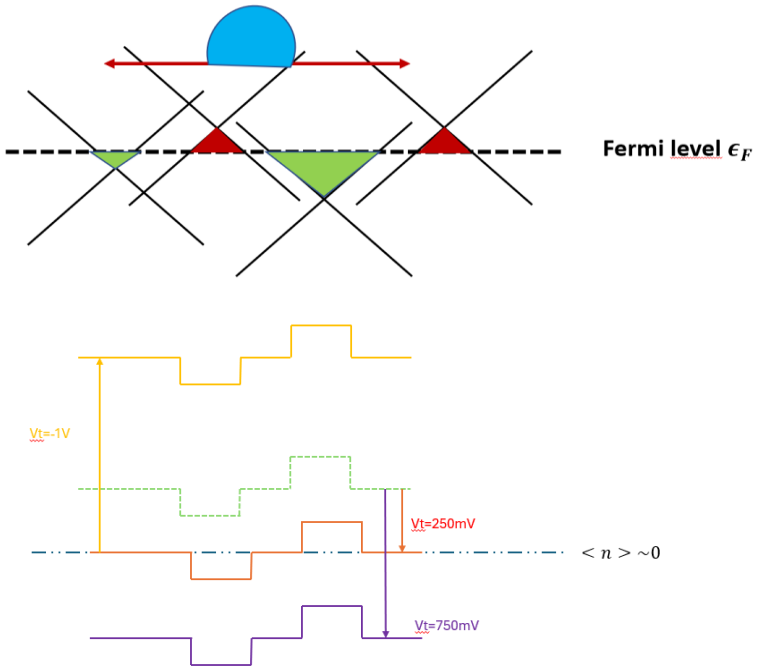

Figure 30 Below a schematic interpretations of the phenomenology observed changing the top liquid gate voltage, while above another possible schematic representation of the "charge impurity potential scenario" through Dirac cones

CONCLUSION AND PERSPECTIVE

In these months I have in particular taken advantage of the great expertise of Mathieu Lizée following his experimental works with the home made set up of the atomic force microscope and ending up giving a new interpretation to the measurement done, discovering the charge puddles effect from graphene.
In light of gaining more experience on the interplay between graphene and ionic liquid, I had also the opportunity to work with Mathieu analysing the interface between the 2D carbon material and different ionic liquids, performing transport measurement, especially pointing out how the electronic mobility can be affected by the ions of the liquid that at the interface act as new scattering centres. Transport measurement in dry and wet condition by means of a probe stations as well as gate-voltage dependent in-plane spectroscopy have been performed.

These studies, performed using the same CVD graphene transistors developed for the other experiments, are here not reported for sake of time and to give a more uniform picture about the internship work.

Presentation and future development of SLGM

Scanning gate microscopy (SGM) is a standard technique that uses a conductive probe to locally modulate the electrostatic potential of a sample while simultaneously measuring its electrical response, leading to high resolution spatial maps of conductance.
In this study we introduce a new variant of this technique, in which a local gate is realized through an electrolyte double layer (EDL) inside a micropipette manipulated by a macroscopic tuning fork (TF) AFM. Such liquid gating is used for its strong interfacial capacitance values, allowing to reach extremely high carrier density regime, compared to what can be achieved with standard solid gating. This allows us to develop a Scanning Liquid Gate Microscopy (SLGM), yielding a powerful, yet simple and non-invasive probing tool. We apply this new technique to graphene field effect transistors (GFET) in which the mean Fermi level can be easily tuned, and reveal charge puddles signatures.
We highlight the exceptional simplicity and ease of use of out TF-AFM based SLGM. Finally, our preliminary results pave the way to systematic SGM investigations at ultra-high charge doping levels on graphene or semiconductors and could be used as a local probe of supercapacitance effects.
List of next steps in the development of the technique:

- New graphene transistor with patterned SiO2/Si substrate by means of ribbons of different metals or samples with areas of the substrate intentionally highly doped.
- Oxidized tungsten tip moving inside a big droplet of ionic liquid covering the whole area of the graphene transistor to monitor the dynamic of adsorption of ionic species or molecules on graphene
- Use of smaller pipette in order to obtain an higher spatial resolution
- Explore more in the direction of double gating possibilities, in particular decoupling the control of the electric field E through the material and n carrier density (already demonstrated since the individual gate potentials superpose in the 2D crystal)

The big project

All the experiments done during this internship aim to have a first glimpse in the two world of physics that the PhD project then will aim to merge together. Understand how design optical collective excitations in semiconductors materials with controlled sharp resonances in the near infrared range to couple them in the same frequency window of the plasmons of water is one of the main goals, taking advantage of the peculiarity of such semiconductor excitations, really at the surface of the material, and therefore potentially able to “talk” to the fluid at the interface.
The appealing idea is the one of creating electrical current by means of a liquid-flow that realize a hydro-electronic drag effect. This type of coupling, that sees Coulomb and phonon drag phenomena, has been measured for water transport in carbon nanotubes (Secchi, 2016), and in experiments carried out at ENS. However, the energy transfer across liquid-solid interfaces remains unknown and could be largely dependent on the electronic properties of specifically designed materials, that will create new solutions for energy harvesting. This would open the way to ‘non-chemical energy transfer between ions and electrons, as an alternative energy harvesting technology.

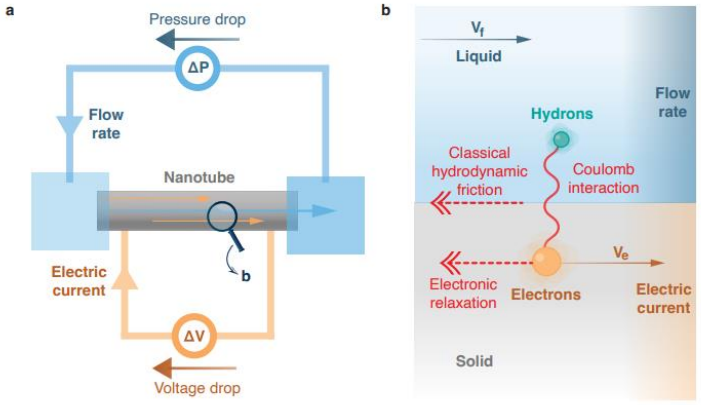

Figure 30 a) sketch of an hydronic generator b) schematic of the momentum transfer and relaxation process at solid-liquid interface from (Coquinot, 2024)

Having in mind this dram the next experiment that will be carried out is the following, using attenuated total internal reflection spectroscopy. The objective would be again to capture an "inter-talking" in between the plasmons of water and the solid, in this case seeing how water can influence the response of the semiconductor's collective mode.

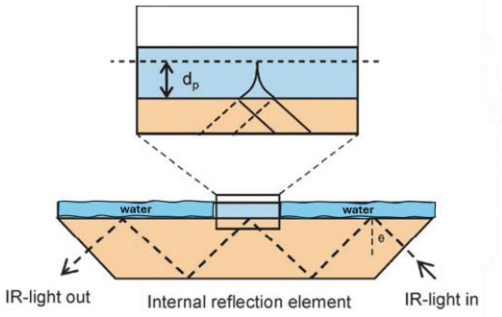

Figure 31 schematic attenuated total internal reflection experiment with insight of the interface evanescent wave (around 100nm)

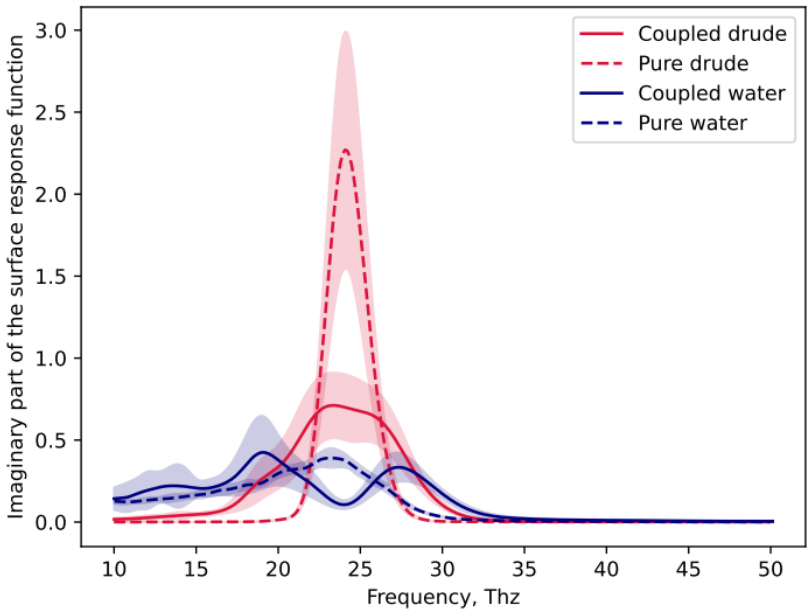

Figure 32 surface response of water dominated by the Debye peak, spanning over three decades in frequency, which results from collective relaxation of molecular dipoles (typical of polar liquids. Numerical simulation of possible coupling between water "hydrons" and semiconductor plasmon. By Damian Toquer (Micromegas ENS team)

Bibliography plasmon semiconductor

Carbon nanotubes flow sensors [Journal] / auth. S.Ghosh. - [s.l.] : Science, 2003.

Charge Puddles in Graphene near the Dirac Point [Journal] / auth. S. Samaddar et all // PHYSICAL REVIEW LETTERS. - 2016.

Charge-induced coherence between intersubband plasmons in a quantum structure [Journal] / auth. A.Delteil A.Vasanelli. - [s.l.] : Physical review letters, 2012.

Cooperative Lamb shift and superradiance in an optoelectronic device [Journal] / auth. G.Frucci. - [s.l.] : New Journal of Physics , 2017.

Experimental study of the dynamical properties of liquid-carbon interface at the nanoscale [Journal] / auth. Marcotte Alice. - [s.l.] : Université Paris sciences et lettres, 2021.

Fast water transport in graphene nanofluidic channels [Journal] / auth. Xie. - [s.l.] : Nature Nanotechnology, 2018.

Fluctuation-induced quantum friction in nanoscale water flows [Journal] / auth. N.Kavokine. - [s.l.] : Nature, 2022.

Generating electricity by moving a droplet of ionic liquid along graphene [Journal] / auth. Guo // Nature Nanotechnology. - 2014.

Hydroelectric energy conversion of waste flows through hydro-electronic drag [Journal] / auth. Coquinot Bapstiste. - [s.l.] : submitted, 2024.

Iontronics - Field effect study of different devices, using techniques of ionic liquid gating [Journal] / auth. J.Seidemann. - [s.l.] : Université Grenoble Alpes, 2017.

Massive radius-dependent flow slippage in carbon [Journal] / auth. Secchi Eleonora. - [s.l.] : Nature, 2016.

Massive radius-dependent flow slippage in carbon nanotubes [Journal] / auth. E.Secchi. - [s.l.] : Nature, 2016.

Measurement of the slip length of water flow [Journal] / auth. Maali. - [s.l.] : Appl.Phys.Lett., 2008.

MicroMegascope based dynamic Surface Force Apparatus [Journal] / auth. all Antoine Lain´et.

Nanotube-Based Biomimetic Ion Pump [Journal] / auth. Rabinowitz. - [s.l.] : Nano Letters, 2020.

Observation of Electron-Hole Puddles in Graphene Using a Scanning Single Electron Transistor [Journal] / auth. J.Martin. - [s.l.] : Nature physics , 2007.

On the role of dynamics in nanoscale liquid transport [Journal] / auth. Lizee Mathieu. - 2024.

Plasmonics: Fundamentals and Applications, page 5, 42-43 [Journal] / auth. A. Stefan. - [s.l.] : Springer US, 2007.

Quantum engineering of collective states [Journal] / auth. Pegoletti Giulia. - 2014 : [s.n.].

Quantum feedback at the solid-liquid interface: flow-induced electronic current and its negative contribution to friction [Journal] / auth. B. Coquinot L. Bocquet, and N. Kavokine. - [s.l.] : Phys Rev X.

Raman Fingerprint of Charged Impurities in Graphene [Journal] / auth. C.Casiraghi. - 2007.

Raman spectroscopy as a versatile tool for studying the properties of graphene [Journal] / auth. M.Basko Andrea C.Ferrari and Denis. - 2013 : Nature Nanotechnology.

Scanning gate microscopy on graphene: charge inhomogeneity and extrinsic doping [Journal] / auth. Jalilian Romaneh. - [s.l.] : Nanotechnology, 2011.

Semiconductor Quantum Plasmonic [Journal] / auth. A.Vasanelli. - [s.l.] : Physical review letters, 2020.

Semiconductor Quantum Plasmonic [Journal] / auth. Haky Andrew. - 2022.

Strong and ultra strong coupling with free-space radiation [Journal] / auth. S.Huppert A.Vasanelli. - [s.l.] : Physical review, 2016.

Superradiant Emission from a Collective Excitation in a Semiconductor [Journal] / auth. T.Laurent Y.Todorov. - [s.l.] : Physical review letters, 2015.

Ultra-strong light–matter coupling for designer Reststrahlen band [Journal] / auth. B.Askenazi. - [s.l.] : New Journal of physics , 2014.

References graphene-liquid

Carbon nanotubes flow sensors [Journal] / auth. S.Ghosh. - [s.l.] : Science, 2003.

Charge Puddles in Graphene near the Dirac Point [Journal] / auth. S. Samaddar et all // PHYSICAL REVIEW LETTERS. - 2016.

Charge-induced coherence between intersubband plasmons in a quantum structure [Journal] / auth. A.Delteil A.Vasanelli. - [s.l.] : Physical review letters, 2012.

Cooperative Lamb shift and superradiance in an optoelectronic device [Journal] / auth. G.Frucci. - [s.l.] : New Journal of Physics , 2017.

Experimental study of the dynamical properties of liquid-carbon interface at the nanoscale [Journal] / auth. Marcotte Alice. - [s.l.] : Université Paris sciences et lettres, 2021.

Fast water transport in graphene nanofluidic channels [Journal] / auth. Xie. - [s.l.] : Nature Nanotechnology, 2018.

Fluctuation-induced quantum friction in nanoscale water flows [Journal] / auth. N.Kavokine. - [s.l.] : Nature, 2022.

Generating electricity by moving a droplet of ionic liquid along graphene [Journal] / auth. Guo // Nature Nanotechnology. - 2014.

Hydroelectric energy conversion of waste flows through hydro-electronic drag [Journal] / auth. Coquinot Bapstiste. - [s.l.] : submitted, 2024.

Iontronics - Field effect study of different devices, using techniques of ionic liquid gating [Journal] / auth. J.Seidemann. - [s.l.] : Université Grenoble Alpes, 2017.

Massive radius-dependent flow slippage in carbon [Journal] / auth. Secchi Eleonora. - [s.l.] : Nature, 2016.

Massive radius-dependent flow slippage in carbon nanotubes [Journal] / auth. E.Secchi. - [s.l.] : Nature, 2016.

Measurement of the slip length of water flow [Journal] / auth. Maali. - [s.l.] : Appl.Phys.Lett., 2008.

MicroMegascope based dynamic Surface Force Apparatus [Journal] / auth. all Antoine Lain´et.

Nanotube-Based Biomimetic Ion Pump [Journal] / auth. Rabinowitz. - [s.l.] : Nano Letters, 2020.

Observation of Electron-Hole Puddles in Graphene Using a Scanning Single Electron Transistor [Journal] / auth. J.Martin. - [s.l.] : Nature physics , 2007.

On the role of dynamics in nanoscale liquid transport [Journal] / auth. Lizee Mathieu. - 2024.

Plasmonics: Fundamentals and Applications, page 5, 42-43 [Journal] / auth. A. Stefan. - [s.l.] : Springer US, 2007.

Quantum engineering of collective states [Journal] / auth. Pegoletti Giulia. - 2014 : [s.n.].

Quantum feedback at the solid-liquid interface: flow-induced electronic current and its negative contribution to friction [Journal] / auth. B. Coquinot L. Bocquet, and N. Kavokine. - [s.l.] : Phys Rev X.

Raman Fingerprint of Charged Impurities in Graphene [Journal] / auth. C.Casiraghi. - 2007.

Raman spectroscopy as a versatile tool for studying the properties of graphene [Journal] / auth. M.Basko Andrea C.Ferrari and Denis. - 2013 : Nature Nanotechnology.

Scanning gate microscopy on graphene: charge inhomogeneity and extrinsic doping [Journal] / auth. Jalilian Romaneh. - [s.l.] : Nanotechnology, 2011.

Semiconductor Quantum Plasmonic [Journal] / auth. A.Vasanelli. - [s.l.] : Physical review letters, 2020.

Semiconductor Quantum Plasmonic [Journal] / auth. Haky Andrew. - 2022.

Strong and ultra strong coupling with free-space radiation [Journal] / auth. S.Huppert A.Vasanelli. - [s.l.] : Physical review, 2016.

Superradiant Emission from a Collective Excitation in a Semiconductor [Journal] / auth. T.Laurent Y.Todorov. - [s.l.] : Physical review letters, 2015.

Ultra-strong light–matter coupling for designer Reststrahlen band [Journal] / auth. B.Askenazi. - [s.l.] : New Journal of physics , 2014.

APPENDIX

Double gating principle

In the set up that we are using we have the opportunity to apply both a back gate and also a top liquid gate. This latter in a transistor can be applied by either a metallic wire dipped in a liquid droplet covering the conducting channel or by a counter electrode placed beside the device. In our case we are using a copper wire inserted in the pippete filled by the liquid.

Electron transport studies have established that electrostatically gating a 2D crystal on both of its surfaces, so-called double gating, using either crystalline dielectrics or liquid electrolytes enables decoupling the control of the electric field E through the material and n carrier density because the individual gate potentials superpose in the 2D crystal. In particular is well-established fact that in double-gated 2D crystals $E \propto V_t - V_b$, whereas n depends only on $V_t + V_b$. Such relation can be understood qualitatively as follows.

Both the two gates can contribute in tuning the graphene's Fermi level, in particular if both of them are fixed at the same potential ($V_t = V_b$), then they will shift the level in the same direction, remembering the proportion relation with $n \propto {E_f}^2$, it can be understood how the sum of these two plays a role. However, the electric fields in the two graphene interfaces (established as gradient of the gate potentials) point in opposite directions in case of equal gating, leading to a zero field across the material. Considering the total opposite case in which the gates are having opposite polarity ($V_t = -V_b$), they will contribute in opposite ways to the density of carriers (shifting the Fermi level in opposite directions, one shift counter-balancing the other), there will be so no induced modification of it, on the contrary the fields at the two interfaces are now pointing in the same direction, resulting in an high electric field inside graphene.